

RESEARCH ARTICLE

# A statistical seasonal forecast model of North Indian Ocean tropical cyclones using the quasi-biennial oscillation

Md Wahiduzzaman<sup>1</sup>  | Eric C. J. Oliver<sup>1,2,3</sup>  | Philip J. Klotzbach<sup>4</sup>  | Simon J. Wotherspoon<sup>1,5</sup>   
Neil J. Holbrook<sup>1,6</sup> 

<sup>1</sup>Institute for Marine and Antarctic Studies, University of Tasmania, Hobart, Tasmania, Australia

<sup>2</sup>Department of Oceanography, Dalhousie University, Halifax, Nova Scotia, Canada

<sup>3</sup>Australian Research Council Centre of Excellence for Climate System Science, Hobart, Tasmania, Australia

<sup>4</sup>Department of Atmospheric Science, Colorado State University, Fort Collins, Colorado, USA

<sup>5</sup>Australian Antarctic Division, Kingston, Tasmania, Australia

<sup>6</sup>Australian Research Council Centre of Excellence for Climate Extremes, Hobart, Tasmania, Australia

**Correspondence**

Md Wahiduzzaman, Institute for Marine and Antarctic Studies, University of Tasmania, Tasmania 7001, Australia.

Email: md.wahiduzzaman@utas.edu.au

**Funding information**

Australian Research Council (ARC), Grant/Award Number: CE170100023; G. Unger Vetlesen Foundation; Tasmania Graduate Research Scholarship, Grant/Award Number: 172141

Previous studies have shown that the skill of seasonal forecasts of tropical cyclone (TC) activity over the North Indian Ocean (NIO) tends to be poor. This paper investigates the forecast potential of TC formation, trajectories and points of landfall in the NIO region using an index of the stratospheric quasi-biennial oscillation (QBO) as the predictor variable in a new statistical seasonal forecast model. Genesis was modelled by kernel density estimation, tracks were fitted using a generalized additive model (GAM) approach with an Euler integration step, and landfall location was estimated using a country mask. The model was trained on 30 years of TC observations (1980–2009) from the Joint Typhoon Warning Center and the QBO index at lags from 0 to 6 months. Over this time period, and within each season and QBO phase, the kernel density estimator modelled the distribution of genesis points, and the cyclone trajectories were then fit by the GAM along the observed cyclone tracks as smooth functions of location. Trajectories were simulated from randomly selected genesis points in the kernel density estimates. Ensembles of cyclone paths were traced, taking account of random innovations every 6-hr along the GAM-fitted velocity fields, to determine the points of landfall. Lead–lag analysis was used to assess the best predictor timescales for TC forecast potential. We found that the best model utilized the QBO index with a 3-month lead. Two hindcast validation methods were applied. First, leave-one-out cross-validation was performed where the country of landfall was decided by the majority vote of the simulated tracks. Second, the distances between the landfall locations in the observations and simulations were calculated. Application of seasonal forecast analysis further indicated that including information on the state of the QBO has the potential to improve the skill of TC seasonal forecasts in the NIO region.

**KEY WORDS**

landfall, North Indian Ocean, quasi-biennial oscillation, statistical modelling, tropical cyclone genesis, tropical cyclone trajectories

## 1 | INTRODUCTION

Tropical cyclones (TCs) are one of the most significant weather hazards in the tropics and represent a major hazard to North Indian Ocean (NIO) rim countries (Alam *et al.*, 2003; Ali *et al.*, 2007; Alam and Collins, 2010; Girishkumar *et al.*, 2012; Mohapatra *et al.*, 2012; Paliwal and

Patwardhan, 2013; Fadnavis *et al.*, 2014; Girishkumar *et al.*, 2014; Mohapatra *et al.*, 2014; Rajasekhar *et al.*, 2014; Girishkumar *et al.*, 2015; Nath *et al.*, 2015). Globally, the impacts of TCs can be devastating, with numerous previous events causing enormous loss of life and property damage, representing significant financial risk to insurance and reinsurance companies (Rumpf *et al.*, 2007). TCs pose multiple

meteorological hazards (e.g., storm surge, heavy rain, strong winds) that can last several days (Ebert *et al.*, 2010). One remarkable example was TC Nargis in 2008, which killed over 135,000 people in Myanmar (Webster, 2008; Lin *et al.*, 2009) and ranked as the second deadliest disaster in the decade from 2000–2009 according to the Centre for Research on Epidemiology of Disasters (Rodriguez *et al.*, 2009). Due to the significant loss of life as well as economic damage caused by TCs making landfall in NIO rim countries (Webster, 2008; Islam and Peterson, 2009; Ng and Chan, 2012; Mohapatra *et al.*, 2014; Pattanaik and Mohapatra, 2016) it is important to assess and anticipate risks as much as possible. Due to the threats that TCs pose to life and property, accurate TC landfall probability forecasts can be potentially beneficial to local populations regarding risks (Tolwinski-Ward, 2015).

Skilful forecasts of TC tracks have particular importance (Fraedrich and Leslie, 1989; Carter and Elsner, 1997; Carson, 1998; Elsner *et al.*, 2006; Camargo *et al.*, 2007; Chu and Zhao, 2007; Basu and Bhagyalakshmi, 2010; Chu *et al.*, 2010; Chand and Walsh, 2011; Balachandran and Geetha, 2012; Camp *et al.*, 2015). In the present study, we have developed a statistical model to better understand and predict NIO region TC activity in the upcoming TC season. The percent contribution of NIO region TCs to the global total differs between studies and time periods investigated, ranging from 5 to 7% (Mohapatra *et al.*, 2014; Schreck *et al.*, 2014; Sahoo and Bhaskaran, 2016) and averaging ~5 TCs per year (Mohapatra *et al.*, 2014). Despite the relatively small percentage of the global total, the socio-economic impacts of TCs in this region are greater than those in other TC basins (Singh, 2010). This is due to the high population density along coastlines in low-lying areas, as well as other physical and socio-economic factors, particularly in Bangladesh (Hossain and Paul, 2017). Furthermore, NIO region TCs are typically characterized by shorter life cycles, and their development relatively close to the coast compared to other basins allows little time for preparation. So, any improvements in TC forecasting for this region can provide significant benefits (Singh *et al.*, 2012).

The quasi-biennial oscillation (QBO) is the primary mode of wind variability in the tropical stratosphere. It represents a quasi-periodic (with a mean phase of 28–29 months) oscillation of the equatorial easterly (E) and westerly (W) zonal winds in the stratosphere (Baldwin *et al.*, 2001). The major features of the QBO are discussed in several papers including Naujokat (1986) and Baldwin *et al.* (2001). We highlight several of these major features below:

- Downwards propagation of easterly and westerly winds in which the propagation of the westerlies is usually faster and more regular than that of the easterlies.
- Transition to easterlies is often delayed between 30 and 50 hPa.

- Easterly anomalies are generally stronger (30–35 m/s) than westerly anomalies (15–20 m/s).
- Highest amplitude of both E and W phases typically occurs near 20 hPa.
- Average periodicity is slightly greater than 2 years.
- Oscillation period and amplitude vary considerably from cycle to cycle.

The circulation of the QBO extends below the tropopause and modulates the amount of water vapour in the air (Zhou *et al.*, 2004; Liang *et al.*, 2011). The QBO has been shown to modulate tropical deep convection (Collimore *et al.*, 2003; Ho *et al.*, 2009; Liess and Geller, 2012), the occurrence of Atlantic hurricanes (Gray, 1984a) and typhoon tracks in the western North Pacific (Ho *et al.*, 2009). Gray (1984a) demonstrated impacts of the QBO on Atlantic TC activity and showed that TC activity in the Atlantic was greater during the QBO westerly phase, or during the transition to the westerly phase, than during the easterly phase. In addition, more major Atlantic hurricanes occurred during westerly QBO years (Gray, 1984b). The QBO effect on Atlantic hurricane activity has been discussed by several authors since Gray's initial publications (Shapiro, 1989; Hess and Elsner, 1994; Landsea *et al.*, 1998; Elsner and Kara, 1999; Arpe and Leroy, 2009). Camargo and Sobel (2010) have also explored the QBO connection with TC activity in the North Atlantic. They found a statistically significant relationship from the 1950s to the 1980s but did not see a significant correlation after the 1980s. Camargo and Sobel (2010) concluded that the QBO–TC frequency relationship was generally weak in most global TC basins. Fadnavis *et al.* (2014) proposed that the phase of the QBO may influence NIO TC trajectories by modulation of tropopause pressure and associated steering winds.

Recently, a potentially useful climatic relationship has been demonstrated between the stratospheric QBO and TC trajectories in the Bay of Bengal (BoB) region of the NIO (Fadnavis *et al.*, 2014). The impact of the QBO on TC trajectories was demonstrated to be stronger during the QBO easterly phase than the QBO westerly phase. Also, the number of TCs was higher during the easterly phase compared to the westerly phase, at least during the more active pre-monsoon and post-monsoon seasons. This follows earlier research work that also proposed relationships between the stratospheric QBO and hurricane activity in the North Atlantic region (Gray *et al.*, 1992; 1994), although the use of the QBO as a predictor for North Atlantic TC activity has been discontinued in recent years (Klotzbach, 2007; Camargo and Sobel, 2010). Other analyses have also tested the effect of the QBO on TC activity in the western North Pacific (Chan, 1995; Baik and Paek, 1998; Lander and Guard, 1998; Ho *et al.*, 2009), the eastern North Pacific (Whitney and Hoggard, 1997), the NIO (Balachandran and Guhathakurta, 1999), the South Indian Ocean (Jury, 1993; Jury *et al.*,

1999) and near northwest Australia (Goebbert and Leslie, 2010).

In the present study, we extend the observational analysis and findings of the QBO–TC relationship by Fadnavis *et al.* (2014) to the entire NIO region, focusing on TC track modulation (as opposed to TC frequency modulation) by the QBO, including modelling this relationship. Specifically, we build and test a statistical seasonal forecast model of NIO region TC formation, tracks and first point of landfall, incorporating the QBO index as the key predictor variable, and compare against climatological model forecasts. Though the overall sample size is small, we believe it is still sufficient for extracting the statistical information necessary for developing the track forecasts. The TC genesis model is built on kernel density estimation (KDE), and a generalized additive model (GAM) projects the average flow trajectories. The organization of this manuscript is as follows: The data and development of model details are depicted in section 2. Modelling of TC genesis distribution by KDE, the GAM for track simulation, and the percentage of landfall probabilities within each country and state are also explained in section 2. In section 3, the prediction and cross-validation outcomes from the model are presented and compared alongside observations. A discussion along with a summary and conclusions are provided in section 4.

## 2 | DATA AND METHODS

Statistical models of TC genesis and track trajectories have been developed in previous studies (Casson and Coles, 2000; James and Mason, 2005; Emanuel, 2006; Rumpf *et al.*, 2007). We adopt a similar approach to that applied by Hall and Jewson (2007) and Yonekura and Hall (2011) for the North Atlantic and western North Pacific Ocean basins, respectively, for our modelling of TC activity in the NIO region. Here we specifically also consider the QBO as a predictor of TC genesis and tracks, excluding the influence of strong El Niño–Southern Oscillation (ENSO) events.

### 2.1 | TC data

TC data were acquired from the Joint Typhoon Warning Center (JTWC) as archived in the International Best Track Archive for Climate Stewardship (IBTrACS) version 6 for the 35-year period from 1979 to 2013 (Knapp *et al.*, 2010). TCs prior to 1979 were excluded from this data set, as there is significant uncertainty in NIO TC genesis and intensity prior to this time (Evan and Camargo, 2010; Weinkle *et al.*, 2012). We define the NIO region to be bounded meridionally from 0° to 30°N and zonally from 50°E to 100°E (Figure 1). The six NIO rim countries (India, Bangladesh, Myanmar, Sri Lanka, Oman and Yemen) that are most strongly affected by TC landfall are considered in this study.

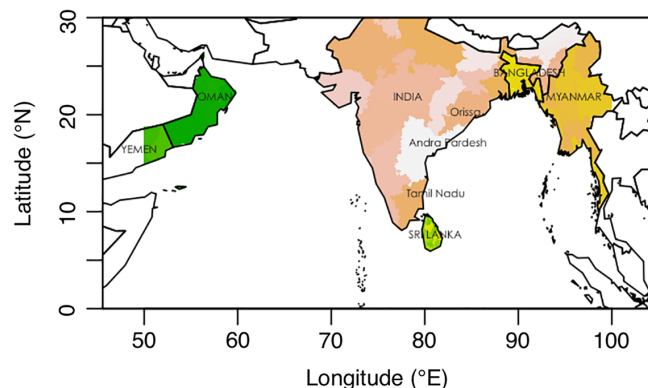


**FIGURE 1** Map identifying the six NIO rim countries (India, Bangladesh, Myanmar, Sri Lanka, Oman and Yemen) and three Indian states (Orissa, Andhra Pradesh and Tamil Nadu) most strongly affected by TC landfalls (reproduced from Wahiduzzaman *et al.*, 2017) [Colour figure can be viewed at [wileyonlinelibrary.com](http://wileyonlinelibrary.com)]

### 2.2 | QBO index

The QBO index is based on a time series of National Centers for Environmental Prediction (NCEP)/National Center for Atmospheric Research (NCAR) Reanalysis zonal mean stratospheric wind shear along the equator ([www.cpc.ncep.noaa.gov/data/indices/qbo.u30/50.index](http://www.cpc.ncep.noaa.gov/data/indices/qbo.u30/50.index)). We have calculated the QBO index as the east–west wind velocity difference between the 30 and 50 hPa levels (i.e., 30 hPa zonal winds minus 50 hPa zonal winds). The QBO index value is computed for every month and season, and the QBO index is then defined to be either in a westerly (W-QBO) or easterly (E-QBO) phase. The easterly phase is defined by a negative QBO index while the westerly phase is defined by a positive QBO index. We have kept our definition consistent with Fadnavis *et al.* (2014). We have also run the model by setting a QBO neutral phase ( $-5 < 0 < 5 \text{ m/s}$ ). When we do this, however, we reduce our already small sample size. Inclusion of the QBO neutral phase does not add further information to our results presented, and there are no significant changes to our results. Consequently, the results in this manuscript do not include a QBO neutral phase. We have separated TC tracks by easterly (E-QBO) and westerly (W-QBO) phase during each TC season.

In keeping with Fadnavis *et al.* (2014), we have also applied two-sample Student's *t*-tests for statistical significance of our analyses. The *t*-test is appropriate as landfall frequency is approximately normally distributed with weak skewness (0.12). Also, the Student's *t*-test deals with the problems associated with inference based on small samples: the calculated mean and standard deviation. We set the null hypothesis that there is no statistically significant relationship between TC landfall frequency and QBO phase. The alternative hypothesis is that there is a statistically significant relationship between TC landfall frequency and QBO phase. To increase the sample size, we have aggregated the NIO region landfall distributions into three zones separated longitudinally. These are (a) 50°–75°E (Arabian Sea region,

including Oman and western India), (b) 75°–90°E (west BoB region, including eastern India, western Bangladesh and Sri Lanka) and (c) 90°–100°E (east BoB region, including eastern Bangladesh and Myanmar).

### 2.3 | Methods

A number of studies have suggested that the QBO has a potentially important influence on TC frequency and tracks (Balachandran and Guhathakurta, 1999; Camargo and Sobel, 2010; Fadnavis *et al.*, 2011; Yadav, 2013; Fadnavis *et al.*, 2014). However, Chan (1995) finds that the relationship between TCs and the QBO does not hold well during strong ENSO events. To increase our sample size and to be consistent with those previous studies, we similarly excluded only strong ENSO events. The years of strong El Niño and La Niña events follow the classification (A 3-month season with an oceanic Niño index) provided by the NOAA Climate Prediction Center (CPC). Nine years were removed from our analysis based on this classification. ENSO events between 1979 and 2009 are listed in Table 1.

Several studies have investigated the frequency and tracks of TCs in the BoB and their relationship with the QBO (Balachandran and Guhathakurta, 1999; Fadnavis *et al.*, 2011; Fadnavis *et al.*, 2014), but no previous study that we are aware of has developed a statistical forecast model to simulate and forecast TC tracks as well as provide probabilistic forecasts of landfall months in advance. Here, we have developed a statistical seasonal forecast model of TC formation, trajectories and landfall in the NIO region for four seasons: winter (December–February), pre-monsoon (March–May), monsoon (June–September) and post-monsoon (October–November), utilizing the QBO as a predictor. The QBO index used in this analysis is smoothed using a 3-month running average, and then a 1 to 6-month lead–lag analysis is performed to assess the best predictor timescale based on TC forecast skill. The model results have been cross-validated (section 2.3.5) and assessed to estimate hindcast skill (section 2.4).

**TABLE 1** Years of strong El Niño and La Niña during the study period (1979–2009), classified by the NOAA CPC based on the oceanic Niño index—the running 3-month mean SST anomaly for the Niño3.4 region (i.e., 5°N–5°S, 120°–170°W)

Year	ENSO event	Year	ENSO event	Year	ENSO event
1979		1990		2000	
1980		1991	Strong El Niño	2001	
1981		1992	Strong El Niño	2002	
1982	Strong El Niño	1993		2003	
1983	Strong El Niño	1994		2004	
1984		1995		2005	
1985		1996		2006	
1987		1997	Strong El Niño	2007	
1988	Strong La Niña	1998	Strong El Niño	2008	
1989	Strong La Niña	1999		2009	Strong El Niño

#### 2.3.1 | TC genesis: KDE

The distribution of genesis points as a function of QBO phase and/or season is approximated by KDE. This approach has been successfully used previously in a variety of studies including those by Vickery *et al.* (2000), James and Mason (2005), Emanuel *et al.* (2006) and Rumpf *et al.* (2007).

KDE is a method to estimate the probability density function (PDF) of a random variable in a nonparametric way. This distribution is defined by a smoothing function and a bandwidth value that controls the smoothness of the resulting density curve.

More formally, kernel estimators convolve each data point with a kernel function  $K$  to produce a smooth estimate  $\hat{f}$  of the density,

$$\hat{f}(x) = \frac{1}{n} \sum_{i=1}^n K\left(\frac{x-x_i}{h}\right).$$

The extent of this contribution is dependent upon the shape of the kernel function and  $h$ , the chosen bandwidth. A larger bandwidth increases the region influenced by each  $x_i$ , resulting in a smoother estimate.

The kernel  $K$  must satisfy the constraint  $\int K(x)dx = 1$ , but is otherwise arbitrary. The Gaussian kernel

$$K(x) = (2\pi)^{-1} \exp\left(-\frac{x^2}{2}\right)$$

is a common choice.

The choice of the bandwidth is a crucial issue for KDE. Bandwidth selection can be performed by “rule of thumb,” by cross-validation, by “plug-in methods” or by other means (Turlach, 1993; Bashtannyk and Hyndman, 2001). The plug-in estimator is derived by writing the density estimate  $\hat{f}$  as a function of the unknown  $f$ , and a pilot estimate of  $f$  is then “plugged in” to derive an estimate of the bias and hence an estimate of the mean integrated squared error. The optimal  $h$  is then chosen to minimize the estimated mean integrated squared error (Loader, 1999).

In this manuscript, the kernel bandwidth has been calculated by a standard plug-in estimator which is an effective

**TABLE 2** For each season and phase, the kernel bandwidth value that have been used in plug-in analysis

Season and phase	Bandwidth value
Easterly phase	7.3
Westerly phase	8
Winter easterly	6.2
Winter easterly	5.5
Pre-monsoon easterly	5.4
Pre-monsoon westerly	6.4
Monsoon easterly	5.6
Monsoon westerly	7.1
Post-monsoon easterly	4.5
Post-monsoon westerly	4.9

method (Rigollet and Vert, 2009). The distribution of genesis points as a function of QBO phase and season is approximated by KDE. In the plug-in analysis, the location density is estimated using KDE where the kernel bandwidth ( $h_{\text{opt}} = 1.06\sigma n^{-1/5}$ , here  $\sigma$ ,  $n$  denote the standard deviation and number of observations, respectively) is not spatially uniform. The bandwidth value for the QBO phases and individual seasons are given in Table 2.

### 2.3.2 | TC tracks: GAM

TC tracks were modelled by fitting a GAM which is a generalization of linear regression (Hastie *et al.*, 2009). In linear regression models, the expected value  $\mu$  of the response or dependent variable  $Y$  is predicted as a linear combination of the predictor variables  $X_1, X_2, \dots, X_p$ ,

$$\mu = E(Y|X_1, X_2, \dots, X_p) = \beta_0 + \beta_1 X_1 + \beta_2 X_2 + \dots + \beta_p X_p,$$

where  $\beta_0, \beta_1, \dots, \beta_p$  are regression coefficients to be estimated. In a GAM, the linear terms are changed by smooth alterations of the predictors,

$$\mu = E(Y|X_1, X_2, \dots, X_p) = \beta_0 + f_1(X_1) + f_2(X_2) + \dots + f_p(X_p).$$

Hence, where linear regression estimates the regression coefficients  $\beta_0, \beta_1, \dots, \beta_p$ , the GAM estimates the smooth transformations  $f_1, f_2, \dots, f_p$ . The GAM application in the present paper is based on the approach used to model the TC climatology for the same region, as discussed in Wahiduzzaman *et al.* (2017).

### 2.3.3 | Landfall locations

We considered the first point of TC landfall for this analysis as multiple landfalls in the NIO region are rare (Evan and Camargo, 2010; Weinkle *et al.*, 2012; Alam and Dominey-Howes, 2015). To determine the positions of landfall, a fine-scale raster mask ( $1/12^\circ$ ) of the NIO rim countries was first constructed. Then, for each TC, we traced along the trajectory to detect the first point (the first time and location crossing of the land mask) where the TC struck land. We also recorded the country and state in which landfall occurred.

### 2.3.4 | Outline for the simulation of TCs

The following outlines the steps that we have undertaken to model TC genesis, tracks and landfall:

1. For each TC observation, the month, season and QBO phase corresponding to TC genesis, together with the month, season and QBO phase corresponding to the track, are calculated.
2. The GAM is fitted to the track increments—it takes as its response the track velocities between successive locations. These velocities are generated by splitting the data by track and calculating the average velocities (in units of degrees of latitude-longitude per day) between successive locations. At higher latitudes (where there are no tracks), there are larger magnitudes of vectors due to having to extrapolate over this part of the study domain but their presence does not affect results.
3. A separate GAM is fitted to each component ( $x, y$ ) of velocity to allow the velocity field to be predicted. In this simple model we fit each velocity as a smooth function of location in each QBO season and phase.
4. The distribution of genesis points is approximated by KDE. The kernel bandwidth is determined automatically using a standard plug-in estimator.
5. Samples are drawn from the estimated density by treating the estimate as a Gaussian mixture (the probability distributions of observations in the overall population)—first a component of the mixture is chosen and then a sample deviate is drawn from that component of the mixture.
6. We restrict genesis to the open ocean by masking the kernel to reject points that fall above a critical depth—here, we choose a critical depth of 200 m, to exclude genesis close to the coast. Similarly, when sampling from the estimated kernel density, we reject any sampled points that fall above a critical depth.
7. Random samples of 50 genesis points are chosen from each of the densities. Regardless of season/QBO phase we always generate 50 TCs, so we do not model the seasonal/QBO variation in TC counts but only their spatial distribution and subsequent tracks and landfalls.
8. The trajectories take a matrix of initial points, and an array of stochastic innovations is applied at each time

**TABLE 3** For each lead month, the proportion of simulated TCs that made landfall within 500 km of the observed location. The bold number highlights the best lead based on the percentage of TC landfall

Lead (months)	TC landfall (%)
1	8
2	35
3	<b>68</b>
4	64
5	46
6	31

**TABLE 4** For each QBO predictor lead in months (ahead of the TC season), the observed and simulated number of TCs that made landfall in each country. The bold number highlights the best lead for each country

Country	Observed landfall	Lead month-1	Lead month-2	Lead month-3	Lead month-4	Lead month-5	Lead month-6
India	40	34	63	51	63	49	<b>37</b>
Myanmar	7	45	18	<b>9</b>	0	0	34
Bangladesh	7	<b>3</b>	1	<b>3</b>	1	0	13
Sri Lanka	4	0	1	<b>2</b>	1	8	0
Yemen	0	0	0	3	1	0	0
Oman	3	1	<b>2</b>	8	15	10	1
NON	40	18	16	25	20	<b>34</b>	16

NON = no landfall and/or landfall in other countries that are not considered in this model.

step. Based on the mean vector field predicted by the model, the TC is advanced with time, adding the relevant stochastic innovation at each step to account for the random nature of the vector field. We selected a 7-day life span since approximately 80% of TC lifetimes in the region are less than 7 days (Wahiduzzaman *et al.*, 2017).

9. To determine landfall, a fine-scale raster mask of the countries bordering the genesis region has been constructed, and we trace along each trajectory to detect the first point where the TC strikes land.

### 2.3.5 | Model validation

We have used two validation methods. These are explained below:

#### Validation method 1

Leave-one-out cross-validation (LOOCV) was conducted by deleting individual trajectories one after another. We have removed the entire track of each TC. Then, the trajectories were simulated by fitting the model to the reduced set of data which corresponds to the deleted tracks. For each track we predicted the state/country of landfall by majority vote from the simulated tracks (where the highest percentage of tracks made landfall).

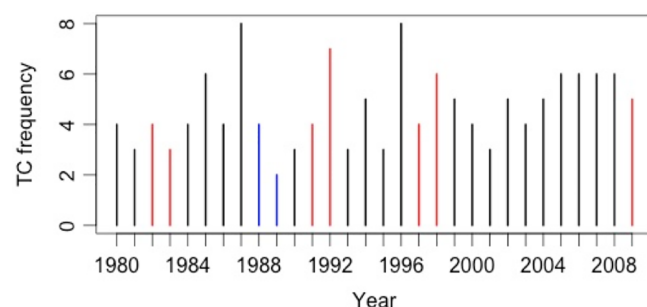


**FIGURE 2** Observed TC frequency (in number) over the NIO ( $0^{\circ}$ – $30^{\circ}$ N and  $50^{\circ}$ – $100^{\circ}$ E) from 1980 to 2009. Black lines indicate years that are considered in this analysis. Red lines show strong El Niño years, and blue lines show strong La Niña years. Strong ENSO events have been excluded from this study [Colour figure can be viewed at [wileyonlinelibrary.com](http://wileyonlinelibrary.com)]

#### Validation method 2

The second validation approach calculates the distance between the observed and simulated landfall points. We remove each track in turn and simulate trajectories from the deleted track based on the reduced data sets. We compute the landfall for the observed tracks for which the TC genesis points are reasonable (>200 m water depth). We measured the distance of the true landfall from the simulated landfall (Wahiduzzaman *et al.*, 2017). For those TCs which did not make landfall in observations (simulations) but made landfall in the simulations (observations), a distance calculation has not been implemented (this is not applicable for the false alarm ratio calculation) since there is no verification data set available. Frequency distributions are then calculated as a function of distance between the simulated and observed landfall locations. The model had an approximately successful TC prediction (false alarm) probability of 80% (20%) which was calculated by considering the relationship between observed and simulated landfalls. This approach considers the standard 2 by 2 contingency table whereby a successful TC prediction (i.e., a ‘hit’) occurs when the forecast event = yes and the observed event = yes. A false alarm occurs when the forecast event = yes and the observed event = no. The probability of a successful TC prediction (false alarm) has been calculated by hits (false alarms)/hits + false alarms.

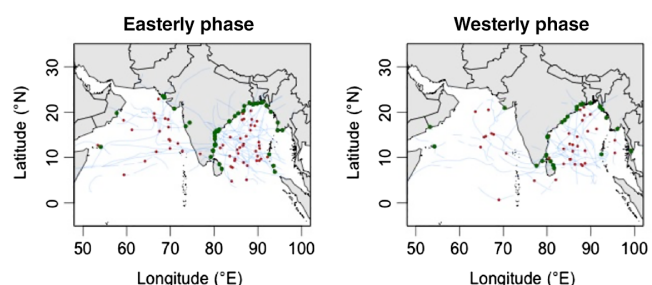


**FIGURE 3** Observed TC genesis, trajectories, and landfall over the NIO ( $0^{\circ}$ – $30^{\circ}$ N and  $50^{\circ}$ – $100^{\circ}$ E) for the easterly (left panel) and westerly (right panel) phases of the QBO from 1980 to 2009. Red dots identify the TC genesis points and blue lines show the TC tracks. The recorded locations of landfall are indicated by green dots [Colour figure can be viewed at [wileyonlinelibrary.com](http://wileyonlinelibrary.com)]

## 2.4 | Best predictor timescale for TC forecast potential

We assessed the best predictor timescale based on a lead–lag analysis from 1 to 6 months. The 3-month lead is based on the central month of the 3-monthly smoothed QBO phase. For example, October–November TC activity uses QBO data from June–July–August. Lead–lag analysis has been performed using two approaches: (a) distance calculation and (b) probability distribution. For each lead–lag period, the percentages of TCs landfall that fell within 500 km of the observed landfall are provided in Table 3. The highest percentage of correctly predicted TC landfalls (68%) is seen for a 3-month lead of the QBO predictor. Though India is contributing the largest portion to total landfalls, the model's performance is not good if we choose a 6-month lead (only 31% simulated landfall matched with observed landfall). The other countries did not perform well using the probability distribution. When considering both approaches, the model performs best with a 3-month lead. We therefore use this 3-month lead for the remainder of our analysis.

We also calculated these results independently for each country (Table 4). Simulations of TC landfall using a 3-month lead QBO predictor compared well against observations and are consistent with the country-independent outcomes shown in Table 4. Our model bias tends to lead to too many landfalls overall for the NIO rim countries. Subtle changes in TC tracks when varying the QBO phase result in too many TCs making landfall in Myanmar except for when a 3-month QBO phase lead is applied.

## 3 | RESULTS

### 3.1 | Genesis and track model fits as a function of QBO phase

A total of 21 years has been considered for analysis here after excluding strong ENSO events. A total of 141 TCs occurred between 1980 and 2009, which is reduced to 101 TCs after excluding strong ENSO years (Figure 2). A total of 58% of months/seasons fall in the easterly QBO phase while the remaining 42% fall in the westerly QBO phase. The increased number of TCs during QBO east years is due to more seasons falling in the easterly QBO phase.

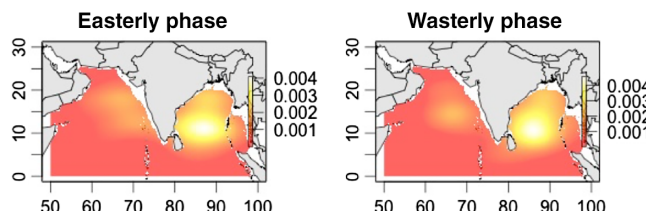


**FIGURE 4** Modelled distributions of TC genesis locations for the easterly (left panel) and westerly (right panel) QBO phases, based on data from 1980 to 2009. The highest density (accumulation of TC frequencies/km<sup>2</sup>) regions for genesis are shown in the yellow colour [Colour figure can be viewed at [wileyonlinelibrary.com](http://wileyonlinelibrary.com)].

We find that landfall frequency is significantly different at the  $p < .05$  ( $>95\%$  confidence level) for the entire NIO basin ( $p = .049$ ) between east and west QBO years. The correlations between landfall frequency and QBO for two cases: all years and excluding ENSO years are weak (0.3) and moderate (0.5).

The observed distribution of TC genesis points depends on the QBO phase (Figure 3). There were 61 (40) genesis points recorded in the easterly (westerly) QBO phase, in keeping with the findings of Fadnavis *et al.* (2014). The presented results that follow also account for the difference in the sample size of QBO-E (58%) and QBO-W (42%) years. TC genesis is relatively even between QBO phases considering their different relative frequency using our QBO definition.

A comparison of the observed TC tracks between the two QBO phases (Figure 3) also shows further differences. Specifically, it is seen that during the easterly QBO phase, more TCs make landfall in the southwestern portion of the BoB (Tamil Nadu and Andhra Pradesh in India), the southwestern part of Bangladesh (Khulna), and along the northwestern part of India (near the Pakistan border). TCs tracking towards Oman across the Arabian Sea are also a more common occurrence in the easterly QBO phase. Conversely, during the westerly QBO phase, 83% of all TCs make landfall in the north and northeastern portions of the BoB, specifically Chittagong in Bangladesh and Myanmar.

The modelled distribution (by KDE) of TC genesis points is shown for each QBO phase in Figure 4. The highest densities are found in the BoB for each phase of the QBO. For both the easterly and westerly QBO phases, the highest density of genesis is seen in the latitudinal range from 8°N

**TABLE 5** Observed total number of TCs that made landfall as a function of QBO phase for each NIO rim country. Individual rows show how landfalls vary by QBO phase for a specific country (%). Individual columns depict how landfalls vary by country for a particular QBO phase (%). Bold percentages show the phase with the highest landfalls for each country and bold italic percentages depict the country with the highest landfalls for each phase

Country	Easterly QBO phase			Westerly QBO phase		
	No	(% <sup>a</sup> )	(% <sup>b</sup> )	No	(% <sup>a</sup> )	(% <sup>b</sup> )
India	25	<b>62.5</b>	<b>41</b>	15	38	<b>37.5</b>
Myanmar	3	43	5	4	<b>57</b>	10
Bangladesh	4	<b>57</b>	6	3	43	8
Sri Lanka	1	25	2	3	<b>75</b>	8
Yemen	0	0	0	0	0	0
Oman	2	<b>67</b>	3	1	33	2
Total landfall	35	57	57	26	43	65
NON <sup>c</sup>	26		43	14		35
Total	61		100	40		100

<sup>a</sup> The difference of landfall frequency by QBO phase for a specific country.

<sup>b</sup> The difference of landfall frequency by country for a particular QBO phase.

<sup>c</sup> No landfall and/or landfall in other countries that are not considered in this model.

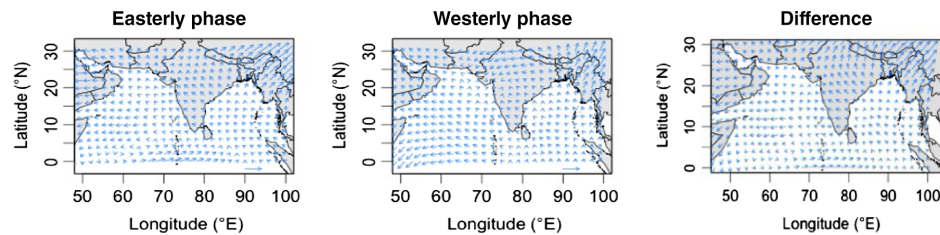


**FIGURE 5** TC track velocities (data from 1980 to 2009) for each QBO phase by fitting the GAM. The velocity magnitude of the reference arrow is 10 m/s [Colour figure can be viewed at [wileyonlinelibrary.com](#)]

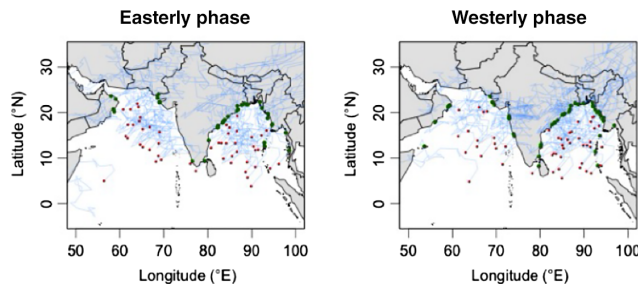


**FIGURE 6** Simulation of TC tracks and landfall as a function of QBO phase. Genesis points were chosen from the modelled kernel. TC genesis points (red colour), TC tracks (blue lines), and first landfall positions (green dots) are also shown [Colour figure can be viewed at [wileyonlinelibrary.com](#)]

to 15°N for the BoB, whereas there is a lower density spatial peaks identifiable in the Arabian Sea for the easterly QBO phase and one in the westerly QBO phase.

Across the NIO rim, the total numbers of TCs that made landfall for each QBO phase are shown for each country in Table 5. A total of 35 TCs made landfall in the easterly QBO phase compared with 26 in the westerly QBO phase. The results show that the largest number of landfalls occurs over India, although we also note that India has the longest coastline of any of the countries in our study region. We normalized landfalls by coastline length [India 7,000 km (6TCs/1,000 km); Myanmar 1,930 km (4TCs/1,000 km); Bangladesh 580 km (12TCs/1,000 km); Sri Lanka 1,340 km

(3TCs/1,000 km); Yemen 1,906 km (0); Oman 2,092 km (2TCs/1,000 km)] and found that the landfall rate is highest for Bangladesh. India's landfall rate is half the landfall rate of Bangladesh when normalized by coastline length. In India, there was a considerably higher overall number of landfalling TCs in the easterly QBO phases (25) compared with the westerly QBO phases (15). All other countries have relatively few TC landfalls overall, so we are unable to draw any robust conclusions on the differences in TC landfalls for other countries based on QBO phases. Two-sample Student's *t*-tests applied on the time series of the number of cyclones for the entire NIO indicate that the landfall frequency is significantly different [at the  $p < .05$  (>95% confidence level)] for the entire basin ( $p = .049$ ) as well as for India ( $p = .042$ ). For other NIO rim countries, no significant differences at the 95% level are observed. This may be due to the small sample size, which is in keeping with the findings of Fadnavis *et al.* (2014).

As discussed in the section 2.3, two-sample Student's *t*-tests applied on the time series of the number of cyclones across three zones indicate that the landfall frequencies between the QBO easterly and westerly phases are statistically significant (90% confidence level) for the eastern part of India, the western part of Bangladesh and Sri Lanka; however, the landfall frequencies for other countries/regions are not significant.

Characterization of the average steering flow direction of cyclones (by fitting the GAM) in each QBO phase is displayed in Figure 5. The GAM model is fitted to track increments—it takes as a response the track velocities between successive locations. These velocities are generated by splitting the data by track and calculating average velocities between successive locations. Though there are no tracks recorded at higher latitudes, there are larger

**TABLE 6** As in Table 5, but for the simulated (bold) total number of TCs that made country landfall in each QBO phase

Country	Easterly phase			Westerly phase		
	No	(%) <sup>a</sup>	(%) <sup>b</sup>	No	(%) <sup>a</sup>	(%) <sup>b</sup>
India	19	54	38	16	46	32
Myanmar	4	40	8	6	<b>60</b>	12
Bangladesh	3	38	6	5	<b>62</b>	10
Sri Lanka	0	0	0	1	<b>100</b>	2
Yemen	0	0	0	0	0	0
Oman	4	<b>67</b>	8	2	33	4
Total landfall	30		60	30		60
NON <sup>c</sup>	20		40	20		40
Total	50		100	50		100

<sup>a</sup> The difference of landfall frequency by QBO phase for a specific country.

<sup>b</sup> The difference of landfall frequency by country for a particular QBO phase.

<sup>c</sup> No landfall and/or landfall in other countries that are not considered in this model.

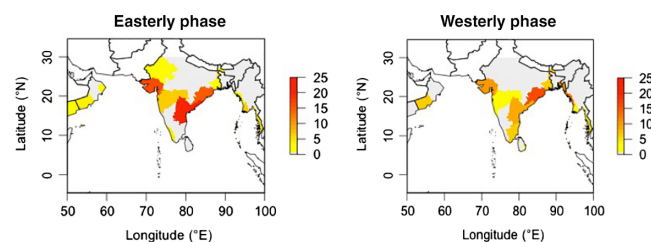


**FIGURE 7** Probabilities of TC landfall (%) by model simulation across the NIO rim states for both QBO phases. Grey indicates that no landfalls are simulated [Colour figure can be viewed at [wileyonlinelibrary.com](#)]

**TABLE 7** As in Table 5, but for the observed total numbers (and percentages) of NIO region TC genesis occurrences as a function of QBO phase for each season

Season	Easterly phase			Westerly phase		
	No	% <sup>a</sup>	% <sup>b</sup>	No	% <sup>c</sup>	% <sup>b</sup>
Winter	12	55	20	10	45	25
Pre-monsoon	12	63	20	7	37	17.5
Monsoon	13	81	21	3	19	7.5
Post-monsoon	24	55	39	20	46	50
Total	61		100	40		100

<sup>a</sup> The difference of landfall frequency by QBO phase for a specific country.

<sup>b</sup> The difference of landfall frequency by country for a particular QBO phase.

<sup>c</sup> No landfall and/or landfall in other countries that are not considered in this model.

magnitudes of vectors due to having to extrapolate over this part of the study domain. These larger velocities (exceeding 10 m/s) are unrealistic (these vectors occur over 0.06% of

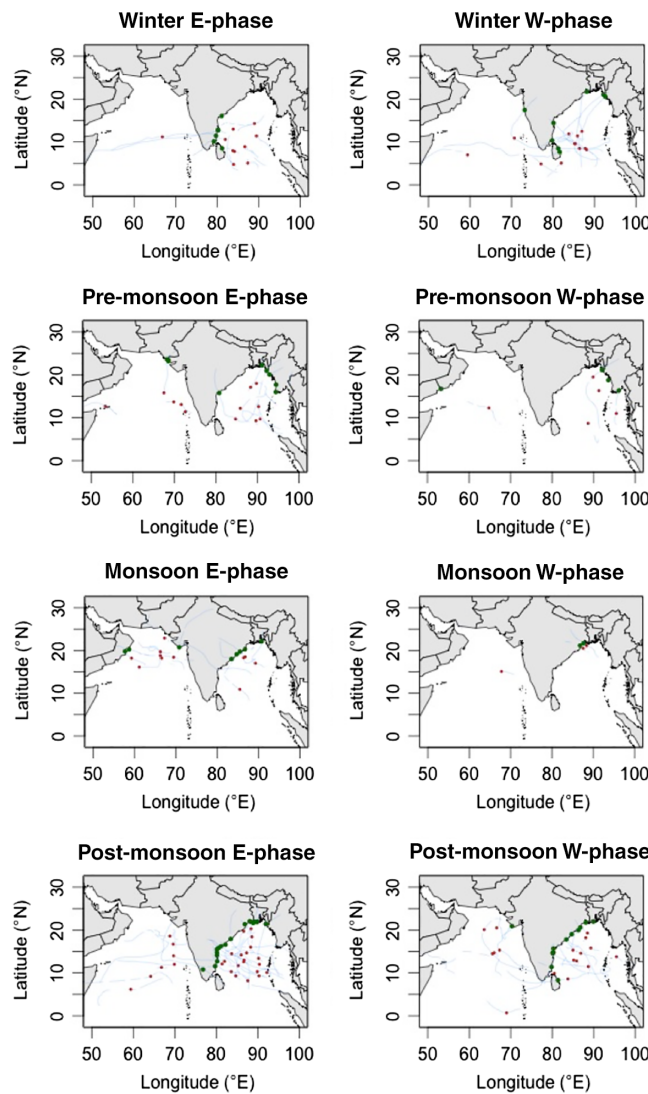


**FIGURE 8** Observed TC genesis, tracks and landfall over the NIO for the easterly QBO phase (E phase) in each of four seasons (left panels), and westerly QBO phase (W phase) in each of four seasons (right panels). Red and green dots identify the TC genesis points and landfall locations, respectively, from 1980 to 2009. Observed TC tracks are shown by blue lines [Colour figure can be viewed at [wileyonlinelibrary.com](http://wileyonlinelibrary.com)]

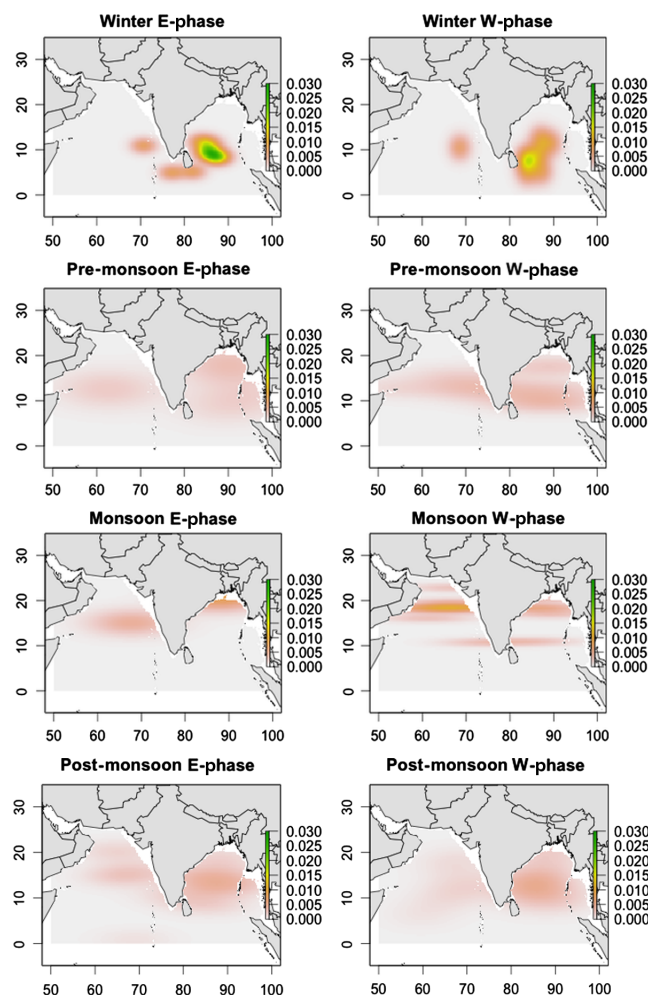


**FIGURE 9** Modelled joint distributions (season and QBO phase) of TC genesis locations based on kernel density estimates of the observed TC genesis occurrences, for both the easterly QBO phase (E phase) (left panels) and westerly QBO phase (W phase) (right panels), based on data from 1980 to 2009. Highest density (accumulation of TC numbers/km<sup>2</sup>) areas of genesis are shown in the green colour [Colour figure can be viewed at [wileyonlinelibrary.com](http://wileyonlinelibrary.com)]

the domain) but their presence does not affect our results since it is polewards from where the TCs are located. During the easterly QBO phase, the velocity field indicates westwards to northwards movement in the BoB. In the Arabian Sea, velocities are mostly westwards with a northwards tendency in the northern portion of the basin. In the westerly QBO phase, the GAM-fitted TC velocity vectors indicate northwards movement over the BoB and mostly northwestwards movement over much of the Arabian Sea.

### 3.2 | Simulated cyclone tracks and landfall locations

Model simulated TC tracks and landfalls are shown in Figure 6. In the easterly QBO phase, TCs tend to track northwestwards with most of them making landfall along the western BoB coast, with 8% more making landfall in India in the easterly QBO phase than in the westerly QBO phase. In the Arabian Sea, Oman and northwest India are modelled

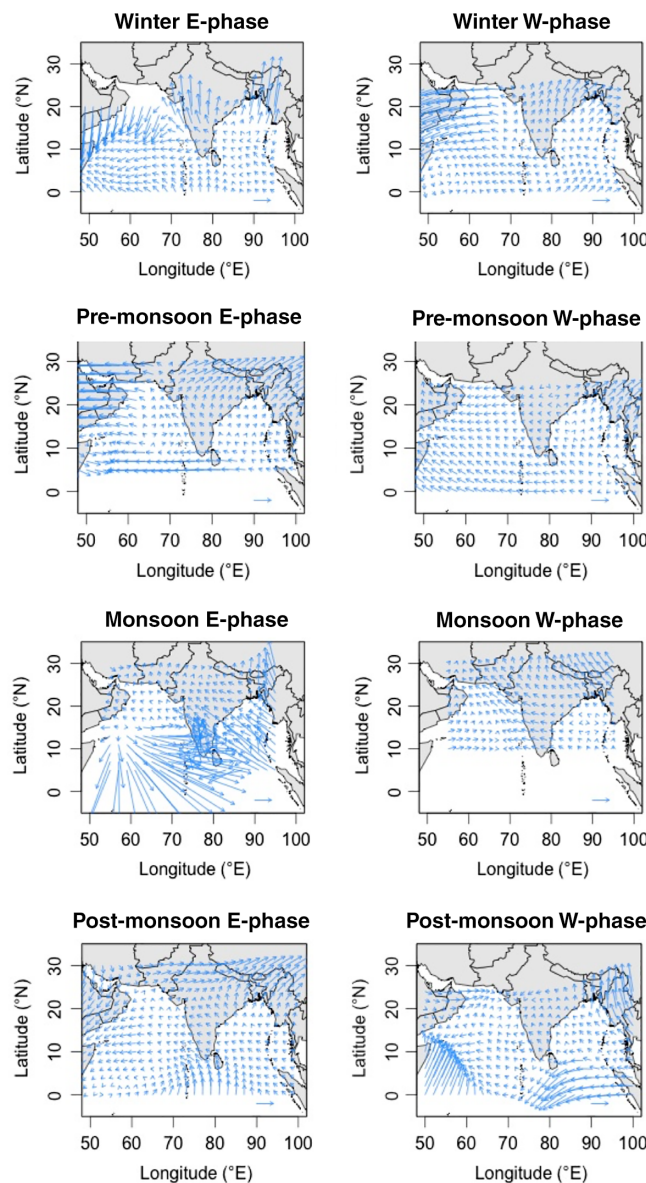


**FIGURE 10** Distribution of GAM-fitted TC track velocities (data from 1980 to 2009) for each QBO phase and season across the North Indian Ocean. The reference arrow velocity magnitude is 10 m/s [Colour figure can be viewed at [wileyonlinelibrary.com](http://wileyonlinelibrary.com)]

to receive the greatest number of landfalls. During the westerly QBO phase, TCs tend to track to the north and northeast over the BoB (Orissa coast in India, Bangladesh and Myanmar). Over the Arabian Sea, TCs tend to travel west with a preferred tendency to make landfall in Oman.

The simulated ratios of TCs that made landfall in each country as a function of QBO phase are specified in Table 6. In the easterly QBO phase, the highest percentage of simulated TC landfall occurrences are in India and Oman. Conversely, during the westerly QBO phase, Bangladesh, Myanmar and Sri Lanka are modelled to have a higher frequency of landfalls. Yemen has no TC landfalls in either QBO phase. Too few TCs have made landfalls in Sri Lanka to make any inferences about statistical significance of the model there. Variations in simulated landfall rates by

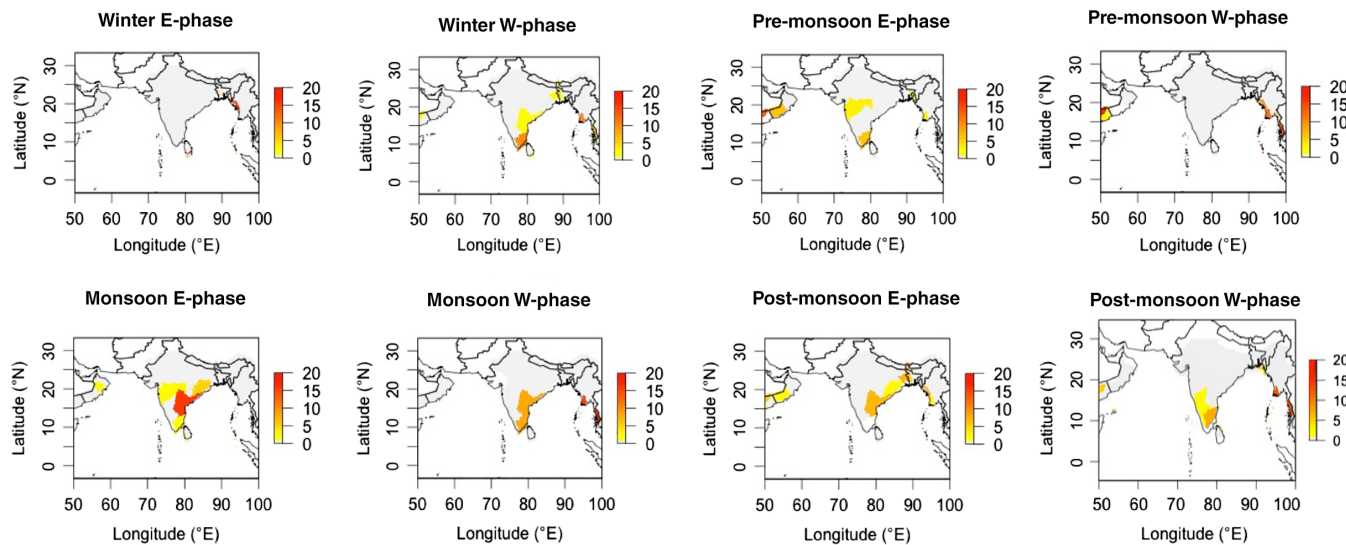
country for a particular QBO phase are also shown in Table 6. In both QBO phases, 60% of simulated TCs made landfall which is close to the observed rate of 61%. The remaining 40% of simulated TCs did not make landfall or made landfall in other countries/islands that are not considered in this model. In the easterly QBO phase, 38% of all simulated TCs made landfall in India with 8% each making landfall in each of Oman and Myanmar, respectively. The simulated landfall rate is 6% in the QBO-E phase for Bangladesh, with no landfalls simulated for Sri Lanka or Yemen. In the QBO-W phase, India was struck by one-third (32%) of the total simulated landfalling TCs. Myanmar received the second highest percentage of simulated landfall occurrences (12%). A total of 10% of the model-simulated TCs made landfall in Bangladesh with 4% making landfall in Oman and 2% making landfall in Sri Lanka.

Figure 7 shows the simulated percentage probabilities of TC landfall for both QBO phases. For the easterly QBO phase, Andhra Pradesh in India is modelled to have the highest percent simulated landfall probability, followed by the state of Orissa in India and then Myanmar. The model produces the maximum percentage probabilities of TC landfall during the westerly QBO phase in Myanmar, followed by Orissa and Andhra Pradesh.

### 3.3 | Genesis and track model fits as a function of both QBO phase and season

The influence of QBO is generally stronger across most NIO region TC seasons during the easterly QBO phase than the westerly QBO phase. The highest genesis rates are seen in the post-monsoon season for both phases of the QBO. In the easterly QBO phases, 39% of genesis occurrences occur in the post-monsoon season, whereas in westerly QBO phases, 50% of genesis occurrences happen in the post-monsoon season. During easterly QBO phases, 21% of genesis occurrences occur in the monsoon season, with both the winter and pre-monsoon seasons accounting for 20% of all genesis events. In westerly QBO phases, 25% of genesis events occur in the winter, followed by the pre-monsoon season (18%). Only 8% of genesis events occur during the monsoon season in the westerly QBO phase (Table 7).

Figure 8 displays how TCs have tracked and where they have made landfall for each season and QBO phase. In the winter season and in the easterly QBO phase, cyclones in the NIO region tended to track westwards, with the majority making landfall along the Tamil Nadu coast in India. In contrast, during the westerly QBO phase, TCs tended to take a northeastwards track over the NIO, with most making landfall in Myanmar. In the pre-monsoon season, TCs tended to track northwards and northeastwards and made landfall in Andhra Pradesh in India and Chittagong in Bangladesh during the easterly QBO phase. During the westerly QBO phase, they tended to track northeastwards and made landfall in southeast Bangladesh as well as Myanmar. In the



**FIGURE 11** Spatial distribution of the percentage probabilities (model simulation) of TC landfall by TC season and QBO phase across NIO rim states and countries [Colour figure can be viewed at [wileyonlinelibrary.com](http://wileyonlinelibrary.com)]

monsoon season, TCs tended to track westwards and made landfall along the Orissa and Gujarat coasts in India as well as Oman during the easterly QBO phase whereas the small number of observed TCs typically tracked west to northwestwards and made landfall in the state of west Bengal in India during the westerly QBO phase. Finally, in the post-monsoon season, TCs were observed to preferentially track northwestwards to make landfall along the Tamil Nadu, Andhra Pradesh and West Bengal coasts in India during the easterly QBO phase, whereas TCs tended to preferentially track northwestwards during the westerly QBO phase and made landfall in Orissa, India and Bangladesh.

The modelled joint distributions (TC season and QBO phase) of TC genesis locations, built on kernel density estimates of the observed TC genesis occurrences recorded in the NIO region, are displayed in Figure 9. The maximum genesis density is located in the BoB during the westerly QBO phase. In the winter season, the highest genesis densities are estimated to be between  $5^{\circ}\text{N}$  and  $14^{\circ}\text{N}$  in the BoB during the easterly QBO phase, while the highest genesis densities are estimated from  $8^{\circ}\text{N}$  to  $11^{\circ}\text{N}$  in the BoB and from  $10^{\circ}\text{N}$  to  $12^{\circ}\text{N}$  in the Arabian Sea during the westerly QBO phase. Genesis tends to take place slightly farther southwest in easterly QBO phases than in westerly QBO phases. In the pre-monsoon season, highest genesis densities are from  $10^{\circ}\text{N}$  to  $15^{\circ}\text{N}$  in the BoB and Arabian Sea during the easterly QBO phase and from  $10^{\circ}\text{N}$  to  $20^{\circ}\text{N}$  during the westerly QBO phase. TCs tend to form closer to the coast in the pre-monsoon season in the westerly QBO phase. In the monsoon season, the highest genesis densities are from  $18^{\circ}\text{N}$  to  $20^{\circ}\text{N}$  in the BoB and  $17^{\circ}\text{N}$  to  $19^{\circ}\text{N}$  for the Arabian Sea in the easterly QBO phase, while the densities are from  $14^{\circ}\text{N}$  to  $16^{\circ}\text{N}$  in the Arabian Sea during the westerly QBO phase. This northwards shift during the monsoon season is due to the large-scale monsoon circulation and associated

position of the monsoon trough. In the post-monsoon season, the highest genesis densities are estimated from  $10^{\circ}\text{N}$  to  $15^{\circ}\text{N}$  in the BoB for both QBO phases and from  $13^{\circ}\text{N}$  to  $15^{\circ}\text{N}$  in the Arabian Sea during the westerly QBO phase. There are more TC genesis events in the Arabian Sea during the easterly phase of the post-monsoon season.

As reported earlier, a GAM was fit to each velocity component of the observed TC tracks to generate a smoother and more complete velocity field over the entire domain. This was undertaken independently for each season and jointly with each phase of the QBO (Figure 10). In the winter season and easterly QBO phase, the fitted velocity field shows the westwards flow field south of  $15^{\circ}\text{N}$  in the BoB and Arabian Sea but the direction changes north of  $15^{\circ}\text{N}$  towards the northeast in the BoB and towards the westnorthwest in the Arabian Sea. In contrast, the fitted velocity field shows a predominantly northwestwards flow field in the BoB south of  $15^{\circ}\text{N}$  before recurring towards the northeast during the westerly QBO phase, while mostly westwards flows are modelled for the Arabian Sea. For the pre-monsoon season, during the westerly QBO phase the flow is mostly northwestwards in the BoB and westwards and less variable in the Arabian Sea whereas the GAM-fitted velocity field shows a mostly northwards flow in the BoB and a westwards flow, albeit highly variable, in the Arabian Sea during the easterly QBO phase. In the monsoon season, the velocity field predominantly shows a northwestwards flow across the NIO region during both QBO phases. In the post-monsoon season, during the easterly QBO phase, westwards flows are mainly seen, except north of  $17^{\circ}\text{N}$  where northwards flow dominates in the BoB. Eastwards flow is seen for the northern portion of the Arabian Sea. In contrast, the GAM-fitted velocity field shows westwards, northwards and northwestwards flow over the BoB and Arabian Sea during the westerly QBO phase in the post-monsoon season.

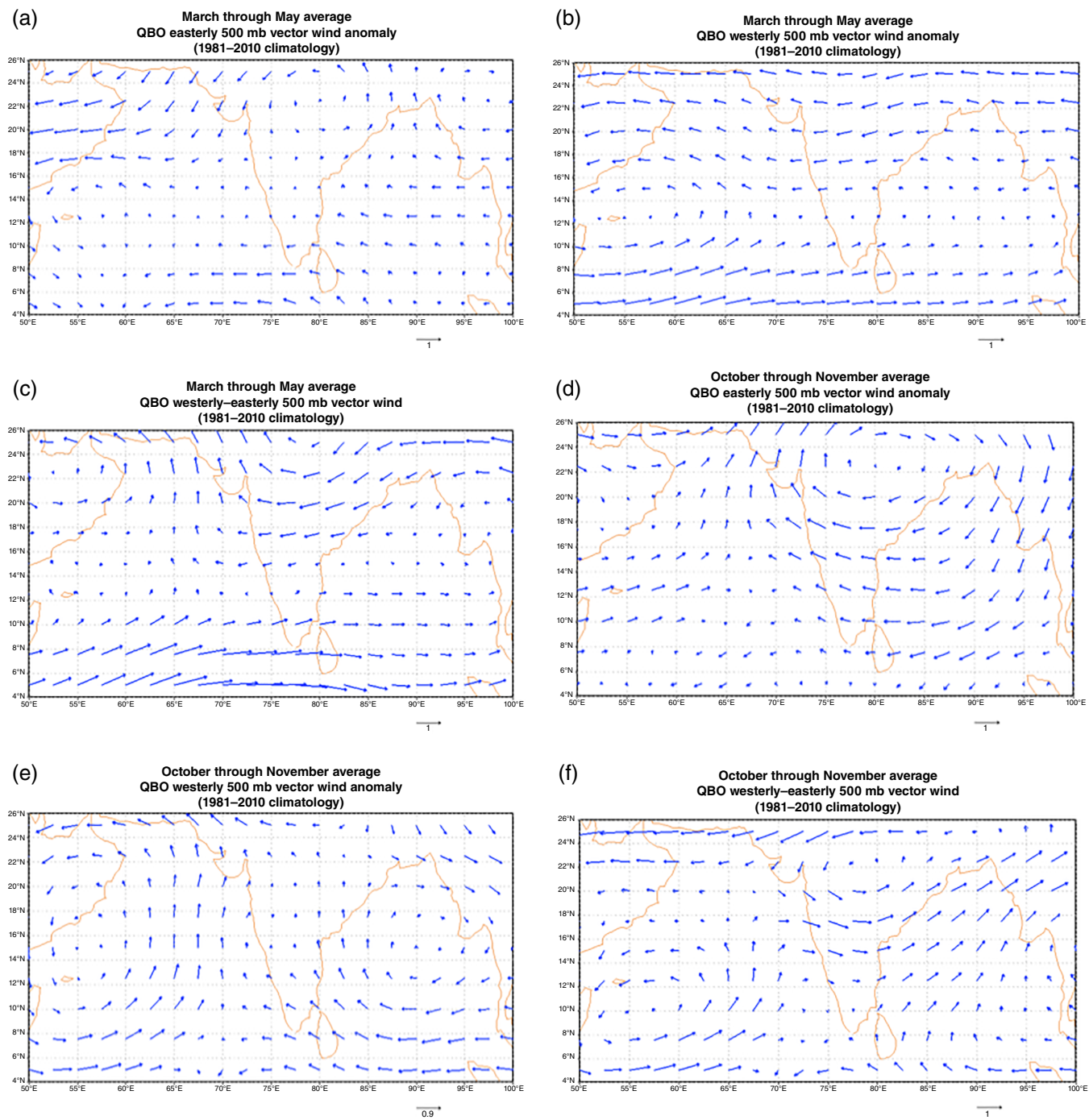


**FIGURE 12** Distribution of 500 hPa winds (m/s) in the pre-monsoon season (March through May) during (a) easterly QBO, (b) westerly QBO and (c) westerly minus easterly QBO, and post-monsoon season (October through November) during (d) easterly QBO, (e) westerly QBO and (f) westerly minus easterly QBO [Colour figure can be viewed at [wileyonlinelibrary.com](http://wileyonlinelibrary.com)]

Simulated TC landfall occurrence percentages as a function of season and QBO phase are shown in Figure 11. During the winter season for both QBO phases, the model predicts the largest probabilities of TC landfalls in Tamil Nadu, India. In the pre-monsoon season, the model simulates Myanmar to have the largest probabilities of TC landfalls during the westerly QBO phase, whereas Gujarat, Andhra Pradesh, Orissa in India, Oman and portions of Bangladesh, are simulated to be the most likely landfall locations in the easterly QBO phase. During the easterly QBO phase and in

the monsoon season, the states of Andhra Pradesh, Orissa and West Bengal in India and Oman have the largest probabilities of simulated TC landfalls, whereas Andhra Pradesh and Orissa in India, Khulna in Bangladesh and Oman experience the largest probabilities TC landfalls in the westerly QBO phase. In the post-monsoon season, the largest probabilities of TC landfall occurrences are seen in the Andhra Pradesh, Tamil Nadu, Orissa and Gujarat states of India during the easterly QBO phase, whereas Andhra Pradesh, Orissa and Tamil Nadu in India are simulated to result in the

**TABLE 8** Total observed and simulated TC landfall occurrences for each north Indian Ocean rim country

Country	Observed number	Simulated number
India	40	51
Myanmar	7	9
Bangladesh	7	3
Sri Lanka	4	2
Oman	3	8
Yemen	0	3
Total landfall	61	76
NON <sup>a</sup>	40	25
Total	101	101

<sup>a</sup> No landfall and/or landfall in other countries that is not considered into model.

largest probabilities of TC landfalls during the westerly QBO phase.

### 3.4 | Dynamical mechanism determining TC movement

The steering flow is the driving force that determines the movement of a TC. The beta effect and air sea interaction also impact the track taken by a TC (Williams and Chan, 1994; Fadnavis *et al.*, 2014). George and Gray (1976) showed that TC motion is best explained by the 500 hPa winds. Chan and Gray (1982) documented the skill of using mid-tropospheric winds for predicting TC tracks. These results were later confirmed by Carr and Elsberry (1990). The influence of QBO phases on steering winds was documented by Fadnavis *et al.* (2014). TC track modulation by the QBO shows the combined effect of QBO-influenced steering winds and the beta effect. Fadnavis *et al.* (2014) used a layer average (850–200 mb) to approximate TC motion. Fadnavis *et al.* (2014) also proposed that the QBO phase might influence TC trajectories through modulations of the tropopause pressure, outgoing longwave radiation (OLR) and steering winds. Furthermore, the QBO modulation of OLR, tropopause pressure and geopotential height and the spatial correlation between the QBO index and OLR indicate linkages between the QBO on TCs via modulation of tropopause pressure, steering winds, OLR and geopotential height (Fadnavis *et al.*, 2014). Here, we examine 500 hPa vector wind anomalies for the pre-monsoon (March–May) and post-monsoon (October–November)

seasons in the NIO for easterly and westerly QBO phases. These two seasons are the most active seasons for TC formation in the NIO.

The steering winds during easterly QBO, westerly QBO and the difference between westerly and easterly QBO phases are shown in Figure 12. In the pre-monsoon season, during the QBO easterly phase, anomalous northeasterly steering winds prevail in the northern portion of the Arabian Sea with generally weaker anomalies farther south in the basin. In the BoB, anomalous southerly flow is evident in the northern portion of the basin, with anomalous easterly flow farther south (Figure 12a). Anomalous easterly flow dominates both the northern portion of the BoB and the Arabian Sea in the QBO westerly phase during the pre-monsoon season, with generally weaker flow farther south in both basins (Figure 12b). The difference between the westerly and easterly QBO phases in the pre-monsoon season highlights westerly flow in the southern portions of both the BoB and Arabian Sea (Figure 12c). In the post-monsoon season, during the easterly phase of the QBO (Figure 12d), anomalous northeasterly flow is evident in the BoB, with predominantly easterly anomalies farther south in the basin. Weaker anomalies are generally evident across the southern portion of the Arabian Sea, with southerly anomalies in the northern portion of the basin (Figure 12d). A pronounced anomalous anticyclone is evident in the 500 hPa steering flow in the westerly phase of the QBO in the post-monsoon season, with anomalous westerly flow in the northern portion of the BoB and anomalous easterly flow in the southern part of the BoB. Anomalous southerly steering flow dominates most of the Arabian Sea (Figure 12e). The difference between the westerly and easterly QBO phases displays southwest winds across the western part of the BoB, highlighting a tendency for TCs to track farther to the northeast in westerly QBO phase episodes during the post-monsoon season (Figure 12f), which is in keeping with the results from the TC track model.

### 3.5 | Validation of model against observations

We validated the model using different methods: (a) LOOCV by a majority vote approach and (b) a distance calculation between observed and simulated landfall. For this QBO forecast model version which contains 101 TCs, the highest number of TC landfalls for observed (40) and predicted landfalls (51) are seen in India. The observed number of landfalls for Myanmar is 7, while the model predicted a total of 9 TC landfalls (Table 8). Overall, the model shows a reasonably good performance.

Again, we calculated the distance between observed landfall and predicted landfall. The distribution of these distances is presented in Figure 13. Due to the random sampling approach adopted here, the frequencies are quite large. Each time we run the model, we remove each track in turn, and simulate multiple trajectories from the modelled genesis

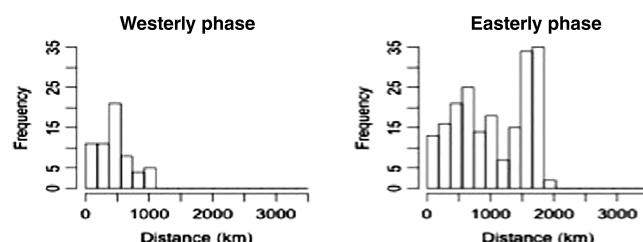


**FIGURE 13** Distribution of distance for simulated landfalls against observed landfall (in number) locations for NIO rim countries

**TABLE 9** Numbers and percentages of annual total observed and simulated (by climatology and QBO predictor) TC landfall occurrences across each country of the NIO rim

Country	Observation		Simulation (climatology)		Simulation (QBO predictor)	
	No	%	No	%	No	%
India	40	39	44	43	51	50
Myanmar	7	7	22	22	9	9
Bangladesh	7	7	0	0	3	3
Sri Lanka	4	4	8	8	2	2
Oman	3	3	6	6	8	8
Yemen	0	0	0	0	3	3
Total landfall	61	60	80	79	76	75
NON <sup>a</sup>	40	40	21	21	25	25
Total	101	100	101	100	101	100

<sup>a</sup> No landfall and/or landfall in other countries that is not considered into model.

point based on the reduced data sets. This produces a large data set. The majority of simulated TC landfalls occurred within 500 km of the observed landfall positions (Figure 13). Given the spatial scale (~1,000 km) of TCs (Harold *et al.*, 1999), landfall within ~500 km of the observations by the model simulation can be considered indicative of good model performance for both QBO phases, noting that there is a peak in the error distribution at ~1,500 km during the easterly QBO phase. A double peak in the climatological NIO TC season (Camargo *et al.*, 2005; Shaevitz *et al.*, 2014; Camp *et al.*, 2015), makes the basin challenging to model. In addition, average 5-day forecast track errors of individual TCs from dynamical models are several hundred kilometres (Mallik *et al.*, 2015; Rayhun *et al.*, 2015). According to Chavas *et al.* (2016), the median storm size (defined by radius to 12 m/s) in the NIO is 287 km, with the global median being about 300 km. The median outer radius of vanishing wind ( $r_0$ ) is closer to 1,000 km. Based on this knowledge of characteristic storm sizes in the NIO, we benchmark our modelled landfall occurrences within ~500 km of the observations as indicative of good model performance for both QBO phases.

### 3.6 | Forecast skill of model measured against observations

A comparison between the percentages of observed and simulated TC landfalls was undertaken to assess the model skill when the predictor is used in model forecasts. The QBO model forecasts represent an improvement in skill over the climatological model forecasts available from Wahiduzzaman *et al.* (2017). The QBO model predicted half of all TCs making landfall (50%) for India, which is close (39%) to observations. Also, the QBO predictor model version predicted landfall for Myanmar (9%) with a similar frequency to observations (7%). Overall, the QBO predictor model gave a 75% probability of TC landfall whereas the observations and climatological model predicted 60 and 79%, respectively (Table 9).

Using the distance calculation approach, 73% of all TC landfalls were within 500 km of the observed landfall positions. For the climatological model, only 63% satisfied the 0–500 km criteria, and consequently the forecast model presented here provides an approximately 25% (skill score =  $\text{score}_{\text{forecast}} - \text{score}_{\text{reference}}/\text{score}_{\text{perfect forecast}} - \text{score}_{\text{reference}} = (73-63)/100-63 = (10/37) = 27\%$ ) improvement over climatology for this error metric (Figure 14).

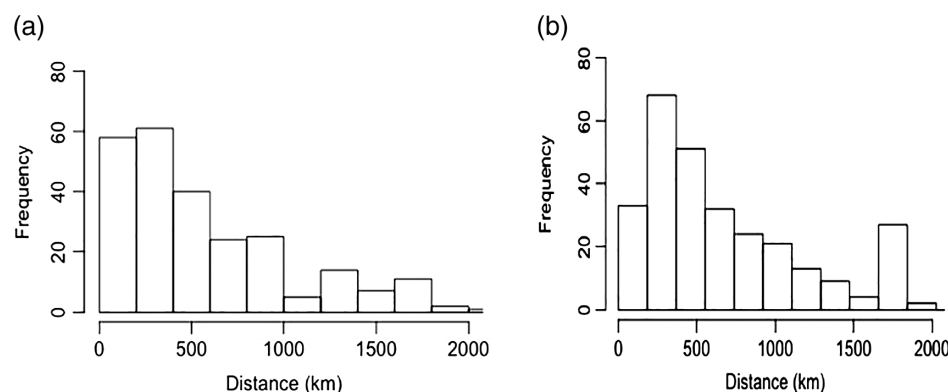


**FIGURE 14** Distribution of distances for simulated landfall against observed landfall (in number) location over the NIO for (a) climatology and (b) climatology plus QBO

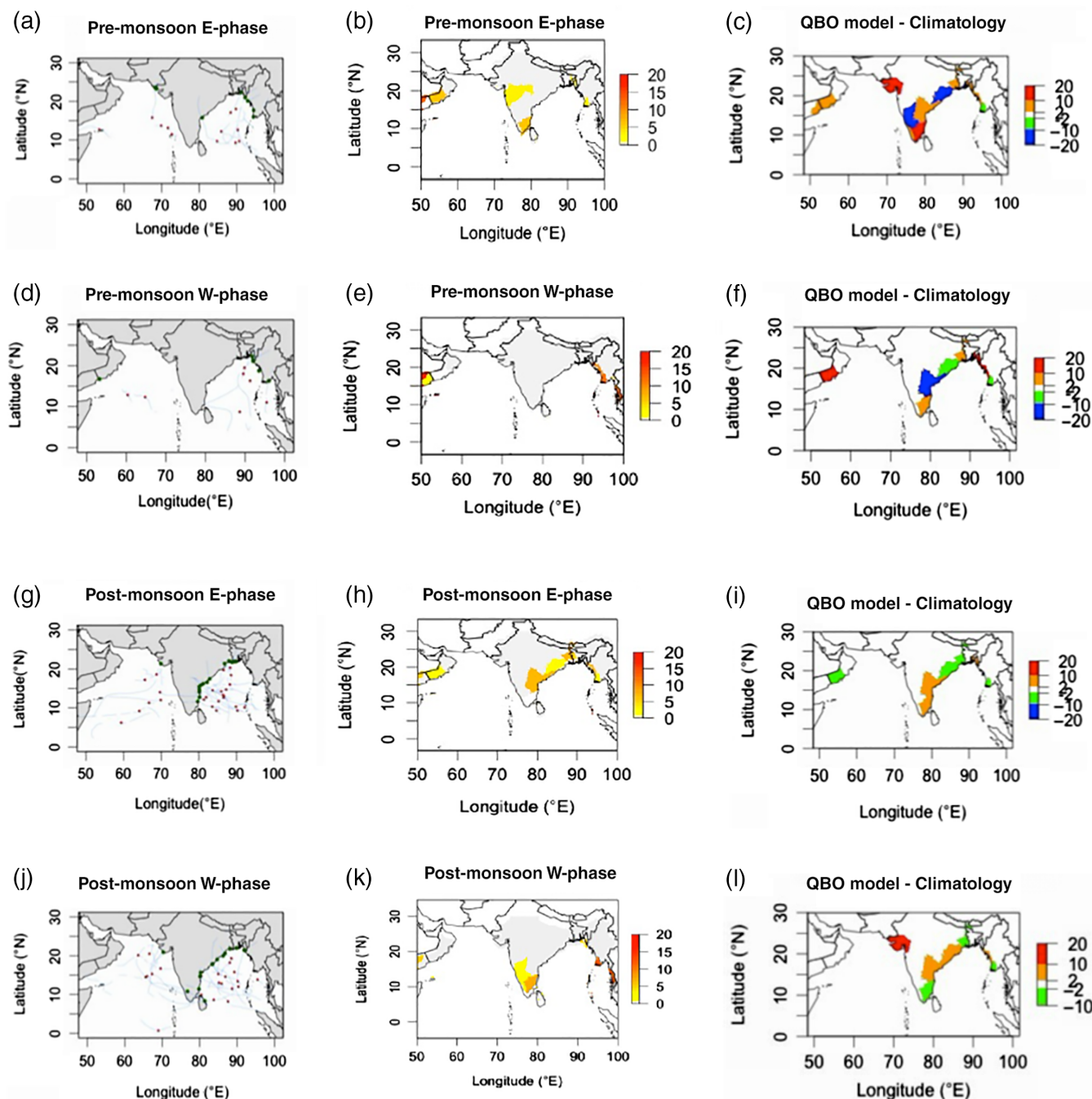


**FIGURE 15** Observed (left), QBO forecast model (middle) and anomalies for the difference between the QBO forecast and climatological model (right) probabilities of landfall (in %) across the north Indian Ocean rim countries ( $0^{\circ}$ – $30^{\circ}$ N and  $50^{\circ}$ – $100^{\circ}$ E) for (a–c) pre-monsoon and QBO easterly phase; (d–f) pre-monsoon and QBO westerly phase; (g–i) post-monsoon and QBO easterly phase; and (j–l) post-monsoon and QBO westerly phase. Results have been aggregated across 30 years of LOOCV [Colour figure can be viewed at [wileyonlinelibrary.com](http://wileyonlinelibrary.com)]

To assess the forecast skill more broadly, we have performed a hold-one-out validation by running the model 30 times, each time holding out 1 year and validating the model based on that held-out year. For example, we held out 1980, fit over 1981–2009, and then predicted 1980. After going through this process 30 times independently, we aggregated the validation statistics by averaging across all of these results to get single maps, by season and QBO phase, showing the landfall probabilities across all years for the QBO forecast model and the change relative to the

climatological model. We have only considered the pre-monsoon and post-monsoon seasons, since they are the peak seasons for TCs. We can see overall that the model forecasts of TC activity for these seasons compare well against the observations. Figure 15 shows, by season and QBO phase, the observations of TC landfall as well as the climatology and forecast model anomalies. During the pre-monsoon easterly phase (Figure 15a), TCs made landfall in Andhra Pradesh and Gujarat in India and Rakhine and Ayeywardy in Myanmar. The QBO model also forecasted well for these

regions (Figure 15b) compared to the climatological model, as seen through the comparison with the anomalies (Figure 15c). In the pre-monsoon westerly phase (Figure 15d), TCs made landfall on the eastern side of the BoB (Chittagong in Bangladesh and Rakhine in Myanmar) and Dofar in Oman (Arabian Sea), and we found that the QBO model predicted a maximum for these regions (Figure 15e) with positive anomalies along these coasts (Figure 15f). The QBO model also predicted higher landfall probabilities in the regions where landfall occurred. During the post-monsoon westerly phase, TCs made landfall in Andhra Pradesh and Tamil Nadu in India and in the south-eastern part of Bangladesh (Figure 15g). The QBO model predicted increased probabilities of landfall for these regions where landfall occurred (Figure 15h,i). In the post-monsoon easterly phase, TCs made landfall along the western side of the BoB (Figure 15j) which was also forecast well by the QBO model (Figure 15k,l). Overall, we found that the skill of the QBO model forecasts of NIO TC landfall is an improvement (25%) over the climatological model.

#### 4 | SUMMARY AND DISCUSSION

The significance of skilful seasonal forecasts is important for many societal sectors and for the framework of developing climate services. In addition, it is valuable among the larger community by increasing the acceptance of climate forecasts (Doblas-Reyes *et al.*, 2013). This study involved the development and evaluation of a statistical seasonal forecast model of TC formation, tracks, and landfall for the NIO region, whereby a form of the stratospheric QBO shear index (30–50 hPa) has been incorporated as the key predictor variable. Fadnavis *et al.* (2014) recently showed that there is a potentially useful climatic relationship between the QBO (excluding medium and strong ENSO years) and TC tracks. Building on their research findings, we applied a GAM approach to fit the observed TC tracks as a smooth background trajectory (flow) field, and as a joint function of QBO phase and TC season. We used a kernel density approach to estimate the distribution of TC genesis points. The kernel bandwidth was calculated with a standard plug-in estimator. Model trajectories were simulated from randomly selected genesis points from the kernel, and are based on the GAM together with an array of stochastic innovations applied at each time step. Two cross-validation methods were also applied. First, LOOCV was performed whereby the country of landfall was chosen using a majority vote approach. The second method involved calculating the distance (as an error metric) between the observed and predicted landfall locations.

During a recent 30-year period (1980–2009), a total of 101 TCs were observed when strong ENSO events are excluded. Of these, 61 (60%) made landfall across the NIO rim countries. We found that the maximum percentage of

TC genesis occurrences was detected in the post-monsoon season for both phases of the QBO. Our model simulations also show that there are significant differences in the directions of the cyclonic trajectories as a function of season and QBO phase that are consistent with the observations. While TC landfall is related to TC intensity, we explored a duration-QBO signal and found the distribution of TC landfall based on duration is not much affected.

The LOOCV analysis showed that the model performed reasonably well for most countries along the NIO rim. The performance of the model was excellent for Myanmar, with relatively good simulation ability for several other countries. However, we do not believe this approach really highlights the value of the forecast model as being an improvement over the climatological model. For that we have used a distance calculation approach. Based on this second cross-validation approach (distance calculation), the majority of modelled TC landfall occurrences were within a relatively short distance (0–500 km) of the observed landfall locations. Given the median TC size (defined by radius to 12 m/s) in the NIO is 287 km, with the global median being about 300 km and compared to the typical error in landfall, this demonstrates that the model is relatively skilful—at least within error estimates characterized by the physical scales of TCs, and typical error scales of dynamical models.

There are many issues with TC data over the NIO prior to 1979 due to lack of geostationary satellite data and limited observations (Evan and Camargo, 2010; Weinkle *et al.*, 2012; Wahiduzzaman *et al.*, 2017). The composites of the mid-level steering flow shown by Fadnavis *et al.* (2014) indicate that the steering flow differences between east and west QBO phases are similar for the pre-1980 and post-1980 periods at mid-levels of the atmosphere. Since the TC tracks are characterized by the steering flow, and the model utilizes this relationship (physical changes in the steering flow exist between east and west QBO events), we fully expect the relationships to be robust on longer periods of data than examined here.

There is currently no available statistical model that utilizes the QBO as a predictor for TCs in the NIO. Consequently, a statistical seasonal forecast model has been considered and developed here and is shown to be successful at forecasting TC tracks. Based on a sensitivity analysis, we chose a predictor time scale of 3 months for the QBO to lead TC activity within each TC season. Overall, our model shows skill exceeding that of climatology for the NIO rim. Also, it shows skill for seasonal forecast from a suite of hindcast simulations. We found that the seasonal forecast model performed with approximately a 25% improvement over the corresponding climatological model. One benefit of this QBO model is the potential for forecasts several months in advance, due to the fairly straightforward downwards propagation of the QBO and its associated high predictability on seasonal timescales.

## ACKNOWLEDGEMENTS

We would like to sincerely thank the anonymous reviewers for their insightful comments that helped us to significantly improve the quality of this manuscript. M.W. was supported by a Tasmania Graduate Research Scholarship (TGRS) for this PhD research undertaken at the University of Tasmania, Hobart, Tasmania, Australia. P.J.K. by a grant from the G. Unger Vetlesen Foundation and N.J.H. by funding from CE170100023.

## ORCID

Md Wahiduzzaman  <https://orcid.org/0000-0002-8974-8247>

Eric C. J. Oliver  <https://orcid.org/0000-0002-4006-2826>

Philip J. Klotzbach  <https://orcid.org/0000-0001-5372-6241>

Neil J. Holbrook  <https://orcid.org/0000-0002-3523-6254>

## REFERENCES

- Alam, E. and Collins, A.E. (2010) Cyclone disaster vulnerability and response experiences in coastal Bangladesh. *Disasters*, 34, 931–954.
- Alam, E. and Dominey-Howes, D. (2015) A new catalogue of tropical cyclones of the northern Bay of Bengal and the distribution and effects of selected landfalling events in Bangladesh. *International Journal of Climatology*, 35, 801–835.
- Alam, M.M., Hossain, M.A. and Shafee, S. (2003) Frequency of Bay of Bengal cyclonic storms and depressions crossing different coastal zones. *International Journal of Climatology*, 23, 1119–1125.
- Ali, M.M., Kishtawal, C.M. and Jain, S. (2007) Predicting cyclone tracks in the north Indian Ocean: an artificial neural network approach. *Geophysical Research Letters*, 34, L04603.
- Arpe, K. and Leroy, S.A.G. (2009) Atlantic hurricanes—testing impacts of local SSTs, ENSO, stratospheric QBO—implications for global warming. *Quaternary International*, 195, 4–14.
- Baik, J.J. and Paek, J.S. (1998) A climatology of sea surface temperature and the maximum intensity of western North Pacific tropical cyclones. *Journal of the Meteorological Society of Japan*, 76, 129–137.
- Balachandran, S. and Geetha, B. (2012) Statistical prediction of seasonal cyclonic activity over north Indian Ocean. *Mausam*, 63, 17–28.
- Balachandran, S. and Guhathakurta, P. (1999) On the influence of QBO over north Indian Ocean storm and depression tracks. *Meteorology and Atmospheric Physics*, 70, 111–118.
- Baldwin, M.P., Gray, L.J., Dunkerton, T.J., Hamilton, K., Haynes, P.H., Randel, W.J., Holton, J.R., Alexander, M.J., Hirota, I., Horinouchi, T., Jones, D.B.A., Kinnersley, J.S., Marquardt, C., Sato, K. and Takahashi, M. (2001) The quasi-biennial oscillation. *Reviews of Geophysics*, 39, 179–229.
- Bashtannyk, D.M. and Hyndman, R.J. (2001) Bandwidth selection for kernel conditional density estimation. *Computational Statistics and Data Analysis*, 36, 279–298.
- Basu, B.K. and Bhagyalakshmi, K. (2010) Forecast of the track and intensity of the tropical cyclone AILA over the Bay of Bengal by the global spectral atmospheric model VARSHA. *Current Science*, 99, 765–774.
- Camargo, S.J. and Sobel, A.H. (2010) Revisiting the influence of the quasi-biennial oscillation on tropical cyclone activity. *Journal of Climate*, 23, 5810–5825.
- Camargo, S.J., Barnston, A.G. and Zebiak, S.E. (2005) A statistical assessment of tropical cyclone activity in atmospheric general circulation models. *Tellus, Series A: Dynamic Meteorology and Oceanography*, 57, 589–604.
- Camargo, S.J., Barnston, A.G., Klotzbach, P.J. and Landsea, C.W. (2007) Seasonal tropical cyclone forecasts. *Bulletin of the World Meteorological Organization*, 56, 297–307.
- Camp, J., Roberts, M., MacLachlan, C., Wallace, E., Hermanson, L., Brookshaw, A., Arribas, A. and Scaife, A.A. (2015) Seasonal forecasting of tropical storms using the Met Office GloSea5 seasonal forecast system. *Quarterly Journal of the Royal Meteorological Society*, 141, 2206–2219.
- Carr, L.E. and Elsberry, R.L. (1990) Observational evidence for predictions of tropical cyclone propagation relative to steering. *Journal of Atmospheric Sciences*, 47, 542–546.
- Carson, D.J. (1998) Seasonal forecasting. *Quarterly Journal of the Royal Meteorological Society*, 124, 1–26.
- Carter, M.M. and Elsner, J.B. (1997) A statistical method for forecasting rainfall over Puerto Rico. *Weather and Forecasting*, 12, 515–525.
- Casson, E. and Coles, S. (2000) Simulation and extremal analysis of hurricane events. *Journal of the Royal Statistical Society, Series C: Applied Statistics*, 49, 227–245.
- Chan, J.C.L. (1995) Tropical cyclone activity in the western North Pacific in relation to the stratospheric quasi-biennial oscillation. *Monthly Weather Review*, 123, 2567–2571.
- Chan, J.C.L. and Gray, W.M. (1982) Tropical cyclone movement and surrounding flow relationships. *Monthly Weather Review*, 110, 1354–1374.
- Chand, S.S. and Walsh, K.J.E. (2011) Forecasting tropical cyclone formation in the Fiji region: a probit regression approach using bayesian fitting. *Weather and Forecasting*, 26, 150–165.
- Chavas, D.R., Lin, N., Dong, W. and Lin, Y. (2016) Observed tropical cyclone size revisited. *Journal of Climate*, 29, 2923–2939.
- Chu, P.-S. and Zhao, X. (2007) A Bayesian regression approach for predicting seasonal tropical cyclone activity over the central North Pacific. *Journal of Climate*, 20, 4002–4013.
- Chu, P.S., Zhao, X., Ho, C.H., Kim, H.S., Lu, M.M. and Kim, J.H. (2010) Bayesian forecasting of seasonal typhoon activity: a track-pattern-oriented categorization approach. *Journal of Climate*, 23, 6654–6668.
- Collimore, C.C., Martin, D.W., Hitchman, M.H., Huesmann, A. and Waliser, D. E. (2003) On the relationship between the QBO and tropical deep convection. *Journal of Climate*, 16, 2552–2568.
- Doblas-Reyes, F.J., García-Serrano, J., Lienert, F., Biescas, A.P. and Rodrigues, L.R.L. (2013) Seasonal climate predictability and forecasting: status and prospects. *Wiley Interdisciplinary Reviews: Climate Change*, 4, 245–268.
- Ebert, E.E., Turk, M., Kusselson, S.J., Yang, J., Seybold, M., Keehn, P.R. and Kuligowski, R.J. (2010) Ensemble tropical rainfall potential (eTRaP) forecasts. *Weather and Forecasting*, 26, 213–224.
- Elsner, J. B. and Kara, A. B. (1999) *Hurricanes of the North Atlantic: Climate and Society*. New York: Oxford University Press.
- Elsner, J.B., Murnane, R.J. and Jagger, T.H. (2006) Forecasting U.S. hurricanes 6 months in advance. *Geophysical Research Letters*, 33, L10704.
- Emanuel, K. (2006) Hurricanes: tempests in a greenhouse. *Physics Today*, 59, 74–75.
- Emanuel, K., Ravela, S., Vivant, E. and Risi, C. (2006) A statistical deterministic approach to hurricane risk assessment. *Bulletin of the American Meteorological Society*, 87, 299–314.
- Evan, A.T. and Camargo, S.J. (2010) A climatology of Arabian Sea cyclonic storms. *Journal of Climate*, 24, 140–158.
- Fadnavis, S., Chakraborty, T., Ghude, S.D., Beig, G. and Ernest Raj, P. (2011) Modulation of cyclone tracks in the Bay of Bengal by QBO. *Journal of Atmospheric and Solar-Terrestrial Physics*, 73, 1868–1875.
- Fadnavis, S., Ernest Raj, P., Buchunde, P. and Goswami, B.N. (2014) In search of influence of stratospheric quasi-biennial oscillation on tropical cyclones tracks over the Bay of Bengal region. *International Journal of Climatology*, 34, 567–580.
- Fraedrich, K. and Leslie, L.M. (1989) Estimates of cyclone track predictability. I: tropical cyclones in the Australian region. *Quarterly Journal of the Royal Meteorological Society*, 115, 79–92.
- George, J.E. and Gray, W.M. (1976) Tropical cyclone motion and surrounding parameter relationships. *Journal of Applied Meteorology*, 15, 1252–1264.
- Girishkumar, M.S., Ravichandran, M. and Pant, V. (2012) Observed chlorophyll-a bloom in the southern Bay of Bengal during winter 2006–2007. *International Journal of Remote Sensing*, 33, 1264–1275.
- Girishkumar, M.S., Thanga Prakash, V.P. and Ravichandran, M. (2014) Influence of Pacific Decadal Oscillation on the relationship between ENSO and tropical cyclone activity in the Bay of Bengal during October–December. *Climate Dynamics*, 44, 3469–3479.
- Girishkumar, M.S., Suprit, K., Vishnu, S., Prakash, V.P.T. and Ravichandran, M. (2015) The role of ENSO and MJO on rapid intensification of tropical cyclones in the Bay of Bengal during October–December. *Theoretical and Applied Climatology*, 120, 797–810.

- Goebbert, K.H. and Leslie, L.M. (2010) Interannual variability of northwest Australian tropical cyclones. *Journal of Climate*, 23, 4538–4555.
- Gray, W.M. (1984a) Atlantic seasonal hurricane frequency, Part I: El Niño and 30 mb quasi-biennial oscillation influences. *Monthly Weather Review*, 112, 1649–1668.
- Gray, W.M. (1984b) Atlantic seasonal hurricane frequency. Part II: forecasting its variability. *Monthly Weather Review*, 112, 1669–1683.
- Gray, W.M., Landsea, C.W., Mielke, P.W., Jr. and Berry, K.J. (1992) Predicting Atlantic seasonal hurricane activity 6–11 months in advance. *Weather and Forecasting*, 7, 440–455.
- Gray, W.M., Landsea, C.W., Mielke, P.W., Jr. and Berry, K.J. (1994) Predicting Atlantic Basin seasonal tropical cyclone activity by 1 June. *Weather and Forecasting*, 9, 103–115.
- Hall, T.M. and Jewson, S. (2007) Statistical modelling of North Atlantic tropical cyclone tracks. *Tellus, Series A: Dynamic Meteorology and Oceanography*, 59, 486–498.
- Harold, J.M., Bigg, G.R. and Turner, J. (1999) Mesocyclone activity over the northeast Atlantic. Part 1: vortex distribution and variability. *International Journal of Climatology*, 19, 1187–1204.
- Hastie, T., Tibshirani, R. and Friedman, J. (2009) *The Elements of Statistical Learning: Data Mining, Inference, and Prediction*. Springer Series in Statistics, 2nd edition. New York: Springer-Verlag, pp. 295–333.
- Hess, J.C. and Elsner, J.B. (1994) Historical developments leading to current forecast models of annual Atlantic hurricane activity. *Bulletin of the American Meteorological Society*, 75, 1611–1620.
- Ho, C.I., Kim, H.S., Jeong, J.H. and Son, S.W. (2009) Influence of stratospheric quasi-biennial oscillation on tropical cyclone tracks in the western North Pacific. *Geophysical Research Letters*, 36, L06702.
- Hossain, M.N. and Paul, S.K. (2017) Simulation of physical and socioeconomic factors of vulnerability to cyclones and storm surges using GIS: a case study. *GeoJournal*, 82(1), 23–41.
- Islam, T. and Peterson, R.E. (2009) Climatology of landfalling tropical cyclones in Bangladesh 1877–2003. *Natural Hazards*, 48, 115–135.
- James, M.K. and Mason, L.B. (2005) Synthetic tropical cyclone database. *Journal of Waterway, Port, Coastal and Ocean Engineering*, 131, 181–192.
- Jury, M.R. (1993) A preliminary study of climatological associations and characteristics of tropical cyclones in the SW Indian Ocean. *Meteorology and Atmospheric Physics*, 51, 101–115.
- Jury, M.R., Pathack, B. and Parker, B. (1999) Climatic determinants and statistical prediction of tropical cyclone days in the southwest Indian Ocean. *Journal of Climate*, 12, 1738–1746.
- Klotzbach, P.J. (2007) Recent developments in statistical prediction of seasonal Atlantic basin tropical cyclone activity. *Tellus, Series A: Dynamic Meteorology and Oceanography*, 59, 511–518.
- Knapp, K.R., Kruk, M.C., Levinson, D.H., Diamond, H.J. and Neumann, C.J. (2010) The international best track archive for climate stewardship (IBTrACS). *Bulletin of the American Meteorological Society*, 91, 363–376.
- Lander, M.A. and Guard, C.P. (1998) A look at global tropical cyclone activity during 1995: contrasting high Atlantic activity with low activity in other basins. *Monthly Weather Review*, 126, 1163–1173.
- Landsea, C.W., Bell, G.D., Gray, W.M. and Goldenberg, S.B. (1998) The extremely active 1995 Atlantic hurricane season: environmental conditions and verification of seasonal forecasts. *Monthly Weather Review*, 126, 1174–1193.
- Liang, C.K., Eldering, A., Gettelman, A., Tian, B., Wong, S., Fetter, E.J. and Liou, K.N. (2011) Record of tropical interannual variability of temperature and water vapor from a combined AIRS-MLS data set. *Journal of Geophysical Research: Atmospheres*, 116, D06103.
- Liess, S. and Geller, M.A. (2012) On the relationship between QBO and distribution of tropical deep convection. *Journal of Geophysical Research: Atmospheres*, 117, D03108.
- Lin, I.I., Chen, C.H., Pun, I.F., Liu, W.T. and Wu, C.C. (2009) Warm ocean anomaly, air sea fluxes, and the rapid intensification of tropical cyclone Narjis (2008). *Geophysical Research Letters*, 36, L03817.
- Loader, C.R. (1999) Bandwidth Selection: classical or plug-in? *Annals of Statistics*, 27(2), 415–438.
- Mallik, M.A.K., Ahsan, M.N. and Chowdhury, M.A.M. (2015) Simulation of track and landfall of tropical cyclone viyaru and its associated storm surges using NWP models. *American Journal of Marine Science*, 3, 11–21.
- Mohapatra, M., Bandyopadhyay, B.K. and Tyagi, A. (2012) Best track parameters of tropical cyclones over the north Indian Ocean: a review. *Natural Hazards*, 63, 1285–1317.
- Mohapatra, M., Bandyopadhyay, B.K. and Tyagi, A. (2014) Status and plans for operational tropical cyclone forecasting and warning systems in the north Indian Ocean region. In: Mohanty, U.C., Mohapatra, M., Singh, O.P., Bandyopadhyay, B.K. and Rathore, L.S. (Eds.) *Monitoring and Prediction of Tropical Cyclones in the Indian Ocean and Climate Change*. Netherlands: Springer.
- Nath, S., Kotal, S.D. and Kundu, P.K. (2015) Seasonal prediction of tropical cyclone activity over the north Indian Ocean using the neural network model. *Atmosfera*, 28, 271–281.
- Naujokat, B. (1986) An update of the observed quasi-biennial oscillation of the stratospheric winds over the Tropics. *Journal of the Atmospheric Sciences*, 43, 1873–1877.
- Ng, E.K.W. and Chan, J.C.L. (2012) Interannual variations of tropical cyclone activity over the north Indian Ocean. *International Journal of Climatology*, 32, 819–830.
- Paliwal, M. and Patwardhan, A. (2013) Identification of clusters in tropical cyclone tracks of north Indian Ocean. *Natural Hazards*, 68, 645–656.
- Pattanaik, D.R. and Mohapatra, M. (2016) Seasonal forecasting of tropical cyclogenesis over the north Indian Ocean. *Journal of Earth System Science*, 125, 231–250.
- Rajasekhar, M., Kishtawal, C.M., Prasad, M.Y.S., Seshagiri Rao, V. and Rajeevan, M. (2014) Extended range tropical cyclone predictions for East Coast of India. In: *Monitoring and Prediction of Tropical Cyclones in the Indian Ocean and Climate Change*. Netherlands: Springer.
- Rayhun, K.M.Z., Quadir, D.A., Chowdhury, M.A.M., Ahsan, M.N. and Haque, M.S. (2015) Simulation of structure, track and landfall of tropical cyclone Bijli using WRF-ARW model. *Journal of Bangladesh Academy of Sciences*, 39, 157–167.
- Rigollet, P. and Vert, R. (2009) Optimal rates for plug-in estimators of density level sets. *Bernoulli*, 15, 1154–1178.
- Rodriguez, J., Vos, F., Below, R. and Guha-Sapir, D. (2009) *Annual Disaster Statistical Review 2008*. Brussels: Centre for Research on the Epidemiology of Disasters (CRED).
- Rumpf, J., Weindl, H., Höppe, P., Rauch, E. and Schmidt, V. (2007) Stochastic modelling of tropical cyclone tracks. *Mathematical Methods of Operations Research*, 66, 475–490.
- Sahoo, B. and Bhaskaran, P.K. (2016) Assessment on historical cyclone tracks in the Bay of Bengal, east coast of India. *International Journal of Climatology*, 36, 95–109.
- Schreck, C.J., Knapp, K.R. and Kossin, J.P. (2014) The impact of best track discrepancies on global tropical cyclone climatologies using IBTrACS. *Monthly Weather Review*, 142, 3881–3899.
- Shaevitz, D.A., Camargo, S.J., Sobel, A.H., Jonas, J.A., Kim, D., Kumar, A., Larow, T.E., Lim, Y.K., Murakami, H., Reed, K.A., Roberts, M.J., Scoccimarro, E., Vidale, P.L., Wang, H., Wehner, M.F., Zhao, M. and Henderson, N. (2014) Characteristics of tropical cyclones in high-resolution models in the present climate. *Journal of Advances in Modeling Earth Systems*, 6, 1154–1172.
- Shapiro, L.J. (1989) The relationship of the quasi-biennial oscillation to Atlantic tropical storm activity. *Monthly Weather Review*, 117, 1545–1552.
- Singh, O.P. (2010) Tropical cyclones: trends, forecasting and mitigation. In: *Natural and Anthropogenic Disasters: Vulnerability, Preparedness and Mitigation*, pp. 256–274. Netherlands: Springer.
- Singh, R., Kishtawal, C.M., Pal, P.K. and Joshi, P.C. (2012) Improved tropical cyclone forecasts over north Indian Ocean with direct assimilation of AMSU-A radiances. *Meteorology and Atmospheric Physics*, 115, 15–34.
- Tolwinski-Ward, S.E. (2015) Uncertainty quantification for a climatology of the frequency and spatial distribution of North Atlantic tropical cyclone landfalls. *Journal of Advances in Modeling Earth Systems*, 7, 305–319.
- Turlach, B.A. (1993) Bandwidth selection in kernel density estimation: a review. *C.O.R.E. and Institut de Statistique*, 19, 1–33.
- Vickery, P.J., Skerlj, P., Steckley, A.C. and Twinsdale, L. (2000) Simulation of hurricane risk in the United States using an empirical storm track modeling technique. *Journal of Structural Engineering*, 126, 1222–1237.
- Wahiduzzaman, M., Oliver, E.C.J., Wotherspoon, S.J. and Holbrook, N.J. (2017) A climatological model of north Indian Ocean tropical cyclone genesis, tracks and landfall. *Climate Dynamics*, 49, 2585–2603.
- Webster, P.J. (2008) Myanmar's deadly daffodil. *Nature Geoscience*, 1, 488–490.
- Weinkle, J., Maue, R. and Pielke, R. (2012) Historical global tropical cyclone landfalls. *Journal of Climate*, 25, 4729–4735.

- Whitney, L.D. and Hobgood, J.S. (1997) The relationship between sea surface temperatures and maximum intensities of tropical cyclones in the eastern North Pacific Ocean. *Journal of Climate*, 10, 2921–2930.
- Williams, R.T. and Chan, J.C.L. (1994) Numerical studies of the beta effect in tropical cyclone motion. Part II: zonal mean flow effects. *Journal of the Atmospheric Sciences*, 51, 1065–1076.
- Yadav, R.K. (2013) Emerging role of Indian ocean on Indian northeast monsoon. *Climate Dynamics*, 41 (1), 105–116.
- Yonekura, E. and Hall, T.M. (2011) A statistical model of tropical cyclone tracks in the western North Pacific with ENSO-dependent cyclogenesis. *Journal of Applied Meteorology and Climatology*, 50, 1725–1739.
- Zhou, X.L., Geller, M.A. and Zhang, M. (2004) Temperature fields in the tropical tropopause transition layer. *Journal of Climate*, 17, 2901–2906.

**How to cite this article:** Wahiduzzaman M, Oliver ECJ, Klotzbach PJ, Wotherspoon SJ, Holbrook NJ. A statistical seasonal forecast model of North Indian Ocean tropical cyclones using the quasi-biennial oscillation. *Int J Climatol*. 2019;39:934–952.  
<https://doi.org/10.1002/joc.5853>